March 2018

Developing a Stable and Selective Non-Enzymatic Electrochemical Glucose Biosensor

Randy A. Melanson
Worcester Polytechnic Institute

Zihao Li
Worcester Polytechnic Institute

Developing a Stable and Selective Non-Enzymatic Electrochemical Glucose Biosensor

A Major Qualifying Project
Submitted to the Faculty of
Worcester Polytechnic Institute
In partial fulfillment of the requirements for the
Degree in Bachelor of Science
In Chemical Engineering

By:

Zihao Li
Randy Melanson

Date: 04/21/2018
Project Advisor
Professor Hong Susan Zhou

Abstract

The goal of this Major Qualifying Project was to develop a stable and sensitive interface architecture for an easy and reusable non-enzymatic electrochemical glucose biosensor. This was achieved by changing the copper oxide nanoparticle morphology that was deposited onto a titanium oxide nanotube array. The interface architecture of the electrode was manipulated by varying the concentration of the equimolar $CuSO_4/H_2SO_4$ solution from 7.8 mM to 250 mM during electrodeposition. Through SEM imaging, cyclic voltammetry scans, and chronoamperometric readings, it was determined that the biosensor interface architecture affected its overall glucose sensing capabilities. The most ideal interface architecture that resulted in the best performing electrochemical glucose biosensor was produced in an electrolyte solution of 50 mM $CuSO_4/H_2SO_4$. At this concentration, the biosensor had a linear glucose sensitivity range from 0.2 to 1.0 mM glucose and had a correlation coefficient of 0.964.

Acknowledgements

This project team would like to thank our advisor, Professor Hong Susan Zhou, for her guidance and support through the completion of this project. Additionally, this team would like to thank the doctoral candidate, Zhiru Zhou, for her assistance and collaboration especially with the SEM imaging.

Table of Contents

Abstract 1

Acknowledgements 2

Table of Contents 3

Table of Figures 5

Chapter 1: Introduction 8

1.1 Electrochemical Glucose Biosensors 8

1.2 Elements of an Electrochemical Glucose Biosensor 9

Chapter 2: Non-enzymatic Interface Architecture 11

2.1 Chemical Stability and Biocompatibility of Titanium Metal 11

2.2 Selective Detection with High Surface Area Titania Nanostructures 12

2.3 Self-Cleaning Applications of Titania for Biosensing 15

2.4 Combining Catalytic Potential of Copper Oxide with Titanium Nanotube Array 15

Chapter 3: Experimental Theory 18

3.1 Titanium Pretreatment 18

3.1.1 Polishing 18

3.1.2 Solvent cleaning 18

3.1.3 Pickling 18

3.2 Electrochemical Techniques 19

3.2.1 Anodic Oxidation 19

3.2.2 Three-electrode Setup 20

3.2.3 Chronoamperometry 21

3.2.4 Cyclic Voltammetry 22

3.3 Analytical Techniques 23

3.3.1 Scanning Electron Microscopy 23

3.3.2 X-ray Diffraction 23

Chapter 4: Experimental Setup 24

4.1 Preparation of TiO_2 Nanotube Array 24

4.2 Preparation of the CuO/TNT Heterostructure 24

4.3 Measurements 24

Chapter 5: Results and Discussion 25

5.1 Synthesizing CuO/TNT Heterostructure by Varying Electrolyte Concentration 25

5.2 Investigating a Broad Electrolyte Concentration Range on Electrode Morphology 27

5.3 Investigating a Broad Electrolyte Concentration Range on Electrode Function 29

5.4 Investigating a Narrow $CuSO_4/H_2SO_4$ Concentration Range on Electrode Function 33

5.5 UV Irradiation Improves Electrode Function 36

5.6 Electrochemical Deposition Techniques Affect Nanoparticle Morphology 38

Chapter 6: Conclusion and Recommendation 39

References 40

Appendix A: Cyclic Voltammograms for Electrodes Synthesized Under Broad Electrolyte Concentration Range 43

Appendix B: Cyclic Voltammograms for Electrodes Synthesized Under Narrow Electrolyte Concentration Range 47

Table of Figures

Figure 1: Elements of a biosensor.....9
Figure 2: Anodization process of titanium metal in electrolyte solution.....12
Figure 3: Sequence of a catalytic reaction.....13
Figure 4: Formation of titanium nanotubes under anodic oxidation in an electrolyte solution containing fluorine.....14
Figure 5: Copper oxide decorated titanium nanotube heterostructure.....16
Figure 6: SEM images of Cu2O particles (a) cubes; (b) Truncated octahedral; (c) Octahedral; and (d) Hexapods with scale bar: 1um. 17
Figure 7: Experimental setup for anodic oxidation.....19
Figure 8: Experimental setup depicting three-electrode cell.....20
Figure 9: Applied waveform for chronoamperometry.....21
Figure 10: Typical voltammogram for chronoamperometry.....21
Figure 11: Applied waveform for cyclic voltammetry. 22
Figure 12: Typical voltammogram for a reversible reaction.....22
Figure 13: Sample SEM image of titanium nanotube array.....23
Figure 14: Titanium foils after anodic oxidation.....25
Figure 15: Oxidized layers formed on the foils after annealing.....26
Figure 16: Copper deposition seen on the titanium foil after chronoamperometry.....26
Figure 17: Successive CuSO4 dilutions during chronoamperometry from left to right and top to bottom highlighting color change.....27
Figure 18: SEM imaging of Cu2O/TNT heterostructures developed using chronoamperometry in an electrolyte solution of CuSO4 and H2SO4 at concentrations of (a) 7.8 mM; (b) 15.6 mM; (c) 31.2 mM; (d) 62.5 mM; (e) 125 mM; and (f) 250 mM.....28
Figure 19: SEM image of the 62.5 mM Cu2O/TNT heterostructure highlighting nanofibers and copper oxide nanoparticle cluster. 28
Figure 20: ImageJ measurements of the nanoparticle diameters as a function of the CuSO4/H2SO4 concentration. 29

Figure 21: Cyclic voltammogram for 15.6 mM electrode in 0.1 M NaOH + 2 mM glucose (blue) and in 0.1 M NaOH (red). Cyclic voltammogram for bare titanium nanotube array in 0.1 M NaOH + 2 mM glucose (green) and in 0.1 M NaOH (purple). 30
Figure 22: Cyclic voltammogram for 125 mM electrode in 0.1 M NaOH + 2 mM glucose (blue) and in 0.1 M NaOH (red). Cyclic voltammogram for bare titanium nanotube array in 0.1 M NaOH + 2 mM glucose (green) and in 0.1 M NaOH (purple). 31
Figure 23: Amperometric measurement of CuO/TNT electrode developed by chronoamperometry with 62.5 mM CuSO4. Response with successive additions of 0.2 mM glucose in 0.10 M NaOH. Inlet is the calibration curve of current response versus glucose concentration. 32
Figure 24: Linear glucose sensing range for CuO/TNT electrode synthesized by chronoamperometry with 62.5 mM CuSO4. 32
Figure 25: Cyclic voltammograms of 50 mM synthesized electrode in 0 mM (light) to 10 mM (dark) glucose solutions. 33
Figure 26: Cyclic voltammograms of 30 mM (blue), 40 mM (red), 50 mM (green), and 60 mM (purple) synthesized electrodes in a 4 mM glucose solution.....34
Figure 27: Amperometric measurement of Cu2O/TNT electrode developed by chronoamperometry with 60 mM CuSO4 (blue) and 50 mM CuSO4 (red). Response with successive additions of 0.2 mM glucose in 0.10 M NaOH. Inlet is the calibration curve of current response versus concentration glucose.....35
Figure 28: Experimental setup for UV irradiation of CuO/TNT heterostructures. 36
Figure 29: Amperometric measurement of 60 mM electrode before UV (blue) and after UV (green), and 50 mM electrode before UV (red) and after UV (purple). Response with successive additions of 0.2 mM glucose in 0.10 M NaOH. Inlet is calibration curve of current response versus glucose concentration.....37
Figure 30: SEM image of electrode synthesized in a 125 mM CuSO4/H2SO4 electrolyte by (a) chronoamperometry, (b) square wave voltammetry with a step potential of 0.005V, (c) square wave voltammetry with a step potential of 0.0024 V. 38
Figure 31: Cyclic voltammogram for blank titanium nanotube array in 2 mM glucose (blue) and in 0 mM glucose (red).....43
Figure 32: Cyclic voltammogram for 7.8 mM CuSO4 + H2SO4 synthesized electrode in 2 mM glucose (blue) and in 0 mM glucose (red).....43

Figure 33: Cyclic voltammogram for 15.6 mM CuSO4 + H2SO4 synthesized electrode in 2 mM glucose (blue) and in 0 mM glucose (red).....44
Figure 34: Cyclic voltammogram for 31.25 mM CuSO4 + H2SO4 synthesized electrode in 2 mM glucose (blue) and in 0 mM glucose (red).....44
Figure 35: Cyclic voltammogram for 62.5 mM CuSO4 + H2SO4 synthesized electrode in 2 mM glucose (blue) and in 0 mM glucose (red).....45
Figure 36: Cyclic voltammogram for 125 mM CuSO4 + H2SO4 synthesized electrode in 2 mM glucose (blue) and in 0 mM glucose (red).....45
Figure 37: Cyclic voltammogram for 250 mM CuSO4 + H2SO4 synthesized electrode in 2 mM glucose (blue) and in 0 mM glucose (red).....46
Figure 38: Cyclic voltammogram for blank (dark blue), 7.8 mM (orange), 15.6 mM (light blue), 31.3 mM (purple), 62.5 mM (green), 125 mM (red), and 250 mM (blue) in 2 mM glucose.....46
Figure 39: 30 mM electrode scanned in 0 mM (dark blue), 2 mM (red), 4 mM (green), 6 mM (purple), 8 mM (light blue), and 10 mM (orange) glucose solutions. 47
Figure 40: 40 mM electrode scanned in 0 mM (dark blue), 2 mM (red), 4 mM (green), 6 mM (purple), 8 mM (light blue), and 10 mM (orange) glucose solutions. 47
Figure 41: 60 mM electrode scanned in 0 mM (dark blue), 2 mM (red), 4 mM (green), 6 mM (purple), 8 mM (light blue), and 10 mM (orange) glucose solutions. 48
Figure 42: Cyclic voltammograms of 30 mM (blue), 40 mM (red), 50 mM (green), and 60 mM (purple) synthesized electrodes in a 0 mM glucose solution.....48
Figure 43: Cyclic voltammograms of 30 mM (blue), 40 mM (red), 50 mM (green), and 60 mM (purple) synthesized electrodes in a 2 mM glucose solution.....49
Figure 44: Cyclic voltammograms of 30 mM (blue), 40 mM (red), 50 mM (green), and 60 mM (purple) synthesized electrodes in a 6 mM glucose solution.....49
Figure 45: Cyclic voltammograms of 30 mM (blue), 40 mM (red), 50 mM (green), and 60 mM (purple) synthesized electrodes in an 8 mM glucose solution.....50
Figure 46: Cyclic voltammograms of 30 mM (blue), 40 mM (red), 50 mM (green), and 60 mM (purple) synthesized electrodes in a 10 mM glucose solution.....50

Chapter 1: Introduction

1.1 Electrochemical Glucose Biosensors

A biosensor is a self-contained, integrated device that is capable of converting biological information into easily processed data. If properly designed, a biosensor could be developed to quickly and accurately display information about the concentration of any given analyte. There are a number of different types of biosensors, but glucose biosensors account for a major portion of the world market. In 2005, approximately 85% of the market for biosensors was dedicated to glucose biosensors and this was estimated to be worth $5 billion.[1] The prevalence and interest in glucose detection is due to the potential impacts that such a device would have on public health and food quality. Glucose detection has been integral for the management of diabetes and could also be groundbreaking for the monitoring of fruit maturation.

Glucose biosensors have already made substantial contributions to the proper management of diabetes for the estimated 422 million diabetics worldwide.[2] These compact electronic devices are able to draw small samples of blood and accurately display the resulting blood glucose concentration. Diabetics must monitor their blood glucose concentrations to properly maintain blood glucose levels. If left unmonitored, blood glucose levels can spike or fall and result in a number of severe complications. In fact, according to the American Diabetes Association, diabetes and improper management is the leading cause of death by disease. Due to current-day glucose biosensors, diabetics have been able to delay and sometimes prevent many health complications. Current-day biosensors, however, are limited to short operational lifetimes because they are designed in the form of disposable strips.

Although disposable biosensors have worked for public health applications, this design is less effective for other industries such as food quality. In the fruit and produce industry, consumers set strict quality standards that can be quantified by glucose levels. When producers do not meet these quality standards, oftentimes there are severe economic consequences.[3] If there were an easy way to ensure fruit quality and proper glucose concentrations, these economic burdens could be avoided. Many methods exist to detect glucose in fruit, but finding a rapid, visual, and inexpensive method of detection is still a great challenge. Current methods include spectrophotometry, HPLC,

gas chromatography, and enzyme kits.[4,5] The current methods have not been developed for widespread commercial use because they are expensive and require laboratory setup. A successful commercial electrochemical glucose biosensor would be accurate, precise, reproducible, and linear over a concentration range of interest. Additionally, the electrochemical glucose biosensor should not be prone to inactivation and it should be small, cheap, portable, and capable of being used by semi-skilled operators.[6] This Major Qualifying Project works toward the development an easy and reusable electrochemical glucose biosensor.

1.2 Elements of an Electrochemical Glucose Biosensor

An electrochemical biosensor consists of different functional parts that work together to convert biological information into electronic signals. In general, an electrochemical biosensor is composed of the interface architecture where the analyte concentration is sensed, the transducer element where current is processed and amplified for electronic signal, and a computer where the signal is translated into meaningful data. Current electrochemical glucose biosensors suffer from instability and short operational lifetimes due to the design of the interface architecture.[7] To prolong the glucose sensor lifetime, the following report works toward developing an improved interface architecture. Figure 1 below shows how these elements of a biosensor work together to transform biological data into electronic signal.

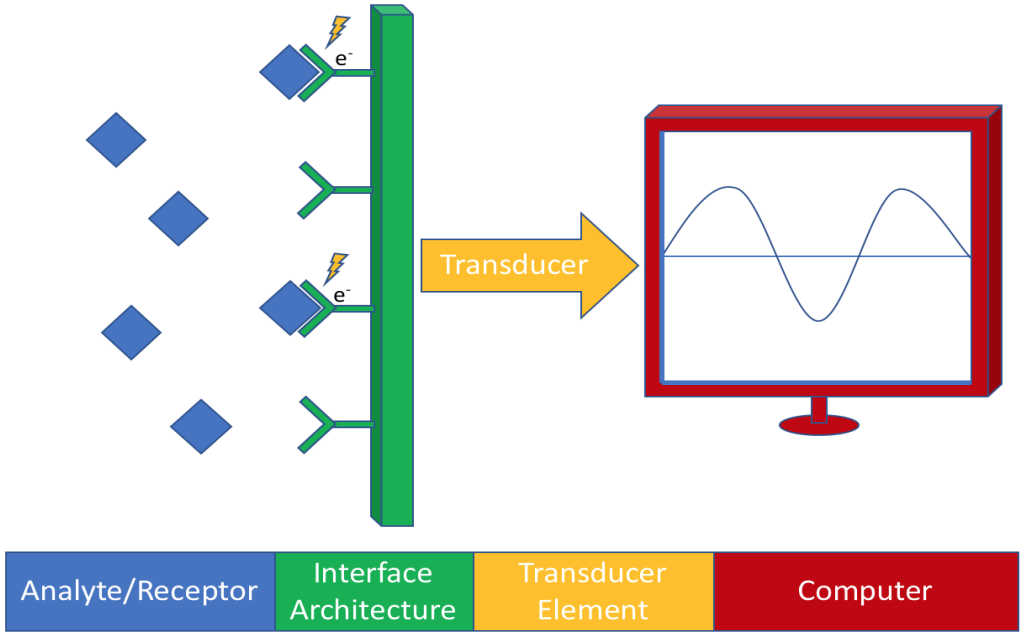

Figure 1: Elements of a biosensor

The interface architecture of electrochemical biosensors traditionally includes immobilized biological recognition elements such as enzymes, nucleic acids, antibodies, etc. These recognition elements can perform highly specific redox reactions that produce measurable current or they can catalyze reactions that produce electroactive species such as H_2O_2. Unfortunately, most biological recognition elements are sensitive to variations in temperature and pH.[7] This instability is problematic because the chemical and physical properties of biofluids can vary greatly which will affect the accuracy of a sensor. For example, a glucose electrochemical biosensor could be used to analyze glucose concentrations in samples ranging from blood and spinal fluid to apples and oranges. These samples have widely different properties that would make traditional biological recognition elements unstable.

To improve the overall stability of electrochemical glucose biosensors, unstable biological recognition elements should be replaced with stable, inorganic catalysts. Most non-enzymatic electrochemical glucose biosensors, however, suffer from an inability to selectively oxidize glucose over other biomolecules. The lack in selectivity results in inaccurate sensing capabilities. To improve the glucose sensitivity, the surface architecture of the electrochemical glucose biosensor must be modified to preferentially catalyze glucose over other biomolecules. The challenge, therefore, is to synthesize the proper inorganic surface architecture that will lead to a stable and selective electrochemical glucose biosensor.

Chapter 2: Non-enzymatic Interface Architecture

2.1 Chemical Stability and Biocompatibility of Titanium Metal

Titanium metal has been implemented in a number of applications within the biomaterials industry. The metal and its related alloys have become prevalent in the industry due to their relative inertness and corrosion resistance. In saline solutions, titanium has a similar corrosion resistance to strong metals such as stainless steel, but it exhibits a lower biological reactivity and does not show enhanced corrosion due to biological media. Due to its stability, corrosion resistance, and metallic strength, titanium has been implemented in many implantable devices and also shows promise for biosensing applications.[8]

Titanium owes its inertness and biocompatibility to the oxide layer that forms on the metal surface. The metal itself it extremely reactive and oxidizes to form titania, TiO_2. Many industries take advantage of the titania layer for its protection against corrosion and for its enhanced adhesive bonding properties. Because the many beneficial qualities of titanium can be attributed to the titania layer, there were attempts to grow relatively thick layers of the oxide. One successful method is called anodic oxidation. Anodic oxidation is a method that applies an electric field to drive the titanium ions, Ti^{4+}, and oxygen ions, O^{2-}, across the oxide film. The migration of each ion species further encourages the growth of the metal oxide film.

Two general reactions occur during the anodic oxidation of titanium metal. The first reaction takes place at the Ti/TiO_2 interface. At this interface, the titanium metal is oxidized to form titanium ions. The second reaction takes place at the TiO_2/electrolyte interface. At this interface, water is reduced to form oxygen ions. The oxygen ions diffuse through the oxide layer due to the electric field and react with the titanium ions to produce titanium oxide. The growing titanium oxide layer reduces the effect of the applied potential and results in a self-inhibiting process.[9] A well-developed titania layer is an essential element for the interface architecture that will contribute to a stable and long-lasting electrochemical glucose biosensor. Figure 2 depicts this process of growing a compact titania layer on titanium metal.

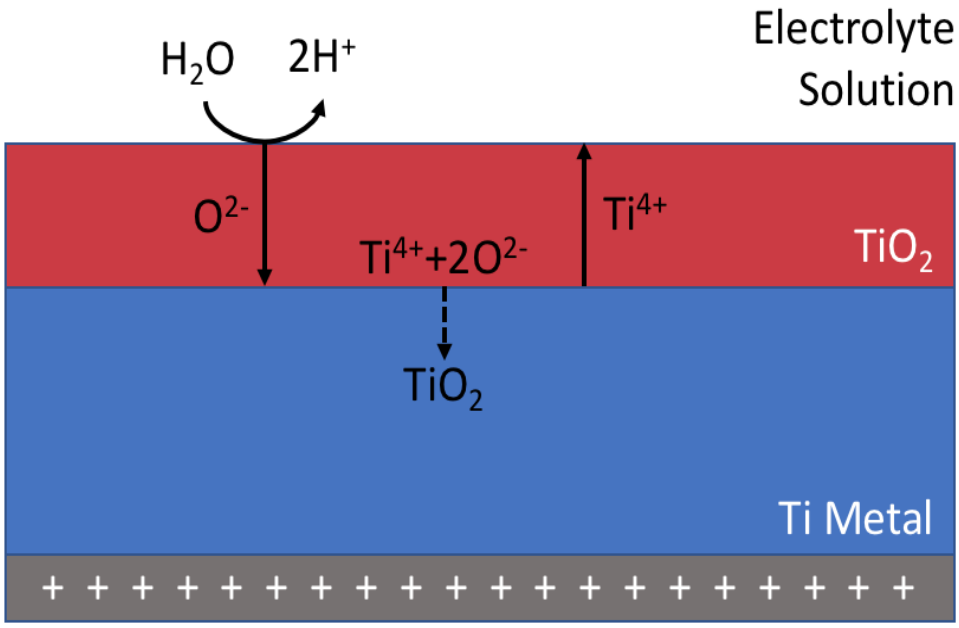

Figure 2: Anodization process of titanium metal in electrolyte solution.

2.2 Selective Detection with High Surface Area Titania Nanostructures

In addition to stability, an effective non-enzymatic electrochemical glucose biosensor must exhibit specificity for glucose catalysis. In biological samples, there are a number of interfering electroactive species such as ascorbic acid (AA), uric acid (UA), and p-acetamidophenol (AP) that can affect sensor specificity. If these electroactive species were catalyzed by the interface architecture, the signal would contain unwanted noise and would result in higher than normal amperometric readings. Fortunately, the catalysis of AA, UA, and AP is subject to diffusion limitations while the catalysis of glucose is subject to kinetic limiations.[10] If the interface architecture is properly designed to reduce kinetic limitations, then the sensor can selectively catalyze the oxidation of glucose over the oxidation of interfering species.

In order to properly design a catalyst that reduces kinetic limitation, the pathway of the analyte must be understood. During catalytic reactions, reactants first diffuse from the bulk fluid to the external surface of the catalyst. After reaching the catalyst surface, the reactant must diffuse to the immediate vicinity of the catalytic active site where it is adsorbed to the surface. Once it is adsorbed onto the surface, the reactant is able to react and form products that follow this process in reverse.[xx] Figure 3 below depicts the described catalytic sequence.

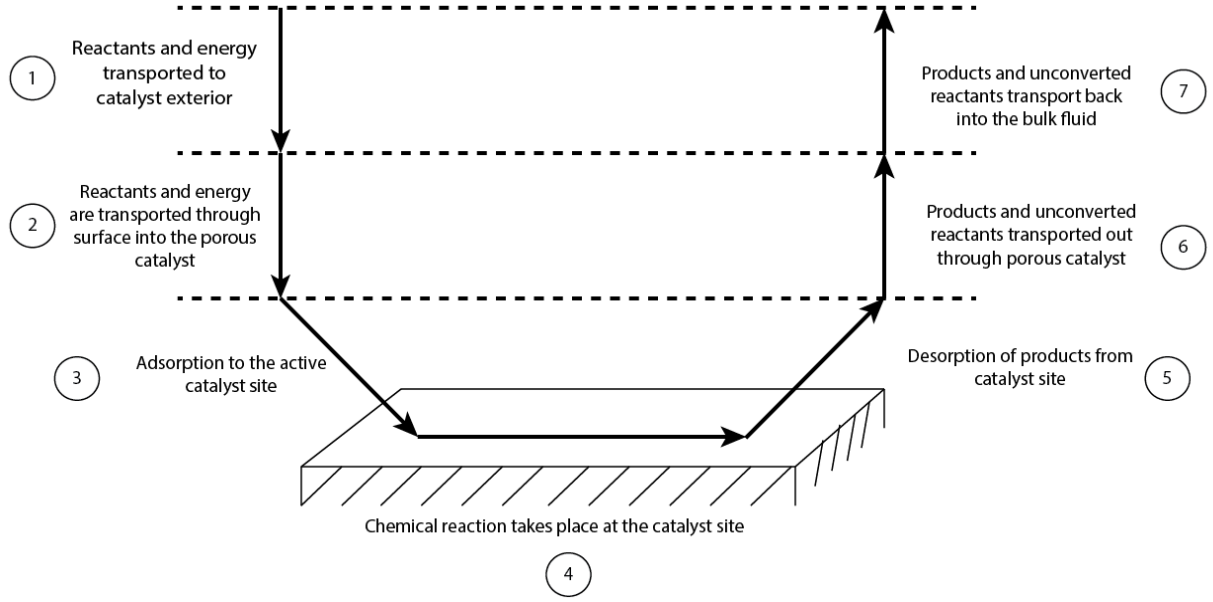

Figure 3: Sequence of a catalytic reaction.

Since diffusion occurs at steps 1 and 2 while reaction kinetics occur at steps 3 and 4, the surface architecture can be tuned to increase reaction kinetics while keeping diffusion relatively constant. Reaction kinetics depend on the ability for the molecule to adsorb to the active site, rearrange its molecular bonds, and desorb to free up the active site for other molecules. One common method to increase reaction kinetics is to increase the number of active sites.[11] This can be done by increasing the total surface area of the catalyst. Thus, an interface architecture with a high surface area should enhance catalysis of glucose while keeping the catalysis of interfering species constant. The overall effect will be a non-enzymatic electrochemical glucose biosensor that can specifically detect glucose in the presence of other electroactive species.

In order to take advantage of the biocompatible features of titania while also specifically catalyzing glucose, a high surface area structure must be synthesized. Although it has been known for many years that titania could form flat, compact layers, recent discoveries have shown that it is also possible to synthesize high surface area titania nanostructures. If fluoride ions are present in the electrolyte during anodic oxidation of titanium, titania nanotubes will be produced rather than a compact oxide layer. The formation of the nanotubes is governed by the competition between

anodic oxide formation and chemical dissolution of the oxide as soluble fluoride complexes. The two general chemical reactions can be represented by:

$$Ti + 2H_2O \rightarrow TiO_2 + 4H^+ + 4e^-$$
$$TiO_2 + 6F^- \rightarrow [TiF_6]^{2-}$$

Under a controlled applied voltage, the O^{2-} and Ti^{4+} ions migrate through the oxide layer and the fluoride ions allow the Ti^{4+} ions to form water soluble complexes. The dissolution of the titanium ions is the mechanism that leads to nanotubes rather than compact oxide layers.[11] The anodic oxidation process is depicted in Figure 4 below.

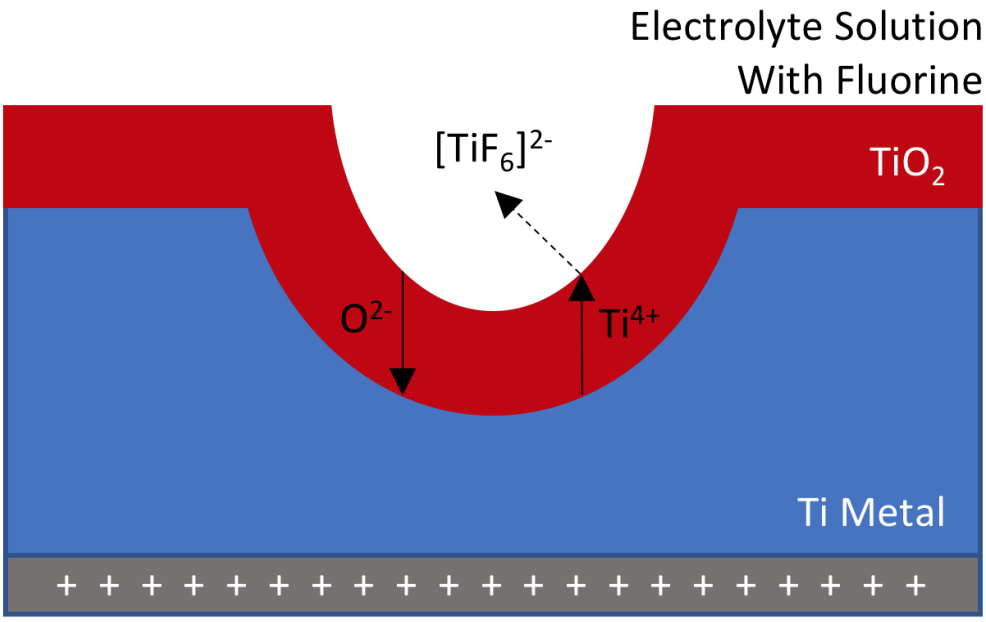

Figure 4: Formation of titanium nanotubes under anodic oxidation in an electrolyte solution containing fluorine.

TiO_2 nanotube arrays exhibit a well-defined geometry, aspect ratio, crystal structure, and biocompatibility.[12,13] This high-surface area, stable scaffold demonstrates a promising design choice for the interface architecture of a non-enzymatic electrochemical glucose biosensor

2.3 Self-Cleaning Applications of Titania for Biosensing

Although titania exhibits durability and chemical stability, it has been shown to interact with biological media by readily adsorbing proteins such as albumin, glycosaminoglycans, collagenase, etc. to form a protein film.[9] The formation of a protein film would likely poison the active sites of the titania layer. Inhibited active sites would drastically reduce the glucose selectivity and operational lifetime of a biosensor. Fortunately, TiO_2 has shown self-cleaning properties due to its ability to maintain highly amphiphilic surfaces upon ultraviolet irradiation. After ultraviolet irradiation the anatase phase of TiO_2 showed a great decrease in water and lipid contact angles.[14] The decrease in liquid contact angle is significant because it suggests that both hydrophilic and hydrophobic contaminants could be removed with water. Easy removal of contaminants would prolong the operational lifetime of the electrochemical sensor.[15] Additionally, the change in wettability was maintained after dark storage and any losses could be recovered by simple exposure to sunlight.[14]

Since titania shows improved wettablility after ultraviolet irradiation, titania nanostructures should similarly exhibit self-cleaning properties. The self-cleaning nature of the TiO_2 nanotube array is an important property for the interface architecture of an electrochemical glucose biosensor because the biosensor functions by oxidizing glucose. After glucose oxidation, many intermediate molecules are formed that adsorb onto the catalyst active sites. To demonstrate the self-cleaning ability of titanium nanotube arrays, an immunoassay with fluorescent proteins was performed.[16] After the assay, the nanotube array was exposed to UV light and washed. It was confirmed that the UV light was able to return the titanium nanotube array to its original conditions using X-ray photoelectron spectroscopy (XPS). After ten cycles of immunoassay testing, the surface of the electrode was fully able to return to its original state.[16] Due to its chemical stability, high surface area, uniform geometry, and self-cleaning properties, the titanium oxide nanotube array was chosen as the scaffold for a reusable and durable electrochemical glucose biosensor.

2.4 Combining Catalytic Potential of Copper Oxide with Titanium Nanotube Array

To convert biological concentrations of glucose into electronic information, glucose molecules must be oxidized. If the oxidation of glucose produces a measurable current, the amplitude of the

current can be related to the analyte concentration. Immobilized enzymes such as glucose oxidase (GOx) and glucose dehydrogenase (GDH) were the conventional choice to perform specific glucose oxidations at the sensing electrode. These enzymes, however are sensitive to temperature ranges and pH fluctuations and would not be effective for a reusable biosensor design.[2] Although titania has exhibited a number of promising biosensor qualities, it does not effectively catalyze the oxidation of glucose. A number of different inorganic catalysts have been studied for glucose oxidation such as platinum and gold nanostructures, silver-graphene composites, and metal oxide species that include cobalt oxide and copper oxide.[17-20]

The copper oxide-based catalysts exhibited a similar catalytic ability for glucose oxidation when compared to the noble metals and is also less expensive. Copper oxide, however, does not easily form high surface area nanostructures. A number of researchers have combined the desirable qualities of the high-surface area titania nanotube array with the catalytic abilities of copper oxide nanoparticles.[21-24] The resulting interface architecture is a glucose sensitive, durable, inorganic heterostructure that shows promise for a reusable electrochemical glucose biosensor. These reports did not, however, synthesize different heterostructure morphologies then subsequently related the surface architecture to the overall glucose sensing capabilities. Figure 5 below illustrates the copper oxide decorated titanium nanotube heterostructure.

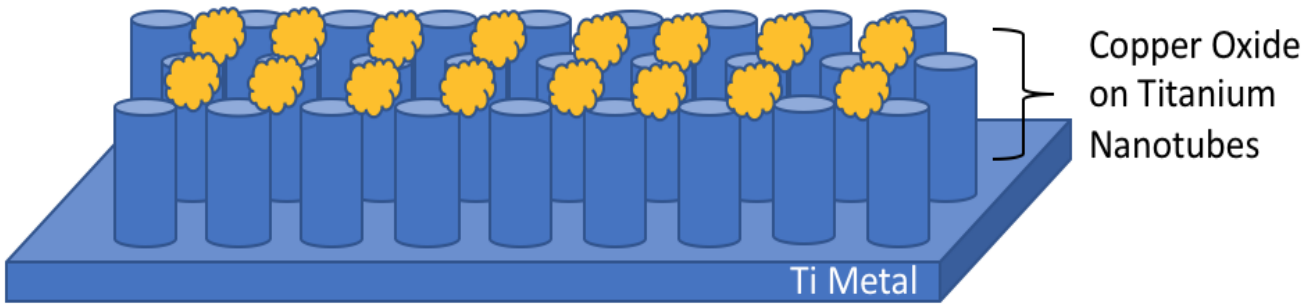

Figure 5: Copper oxide decorated titanium nanotube heterostructure.

In many aspects of nature, morphology is closely related to function. The morphology of the nanoparticles deposited onto the nanotube array would likely affect the overall glucose sensing capability of the heterostructure. There has been extensive interest in synthesizing unique

morphologies of copper oxide nanoparticles so that catalyst morphology can then be related specific electrocatalytic capabilities.[25] Figure 6 below depicts copper oxide particles that were grown to exhibit cubic, octahedron, truncated octahedron, and hexapod morphologies but were not deposited onto titanium nanotube arrays.

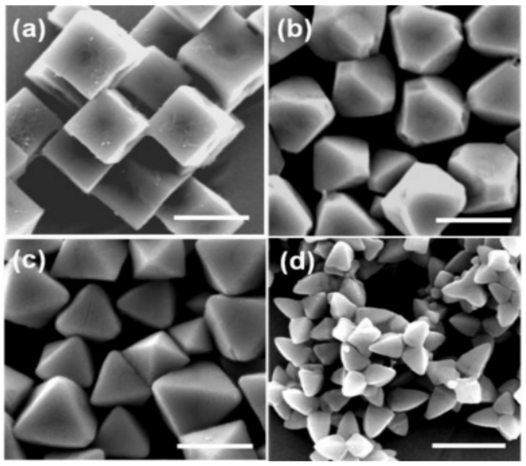

Figure 6: SEM images of Cu2O particles (a) cubes; (b) Truncated octahedral; (c) Octahedral; and (d) Hexapods with scale bar: 1um.

Because the above nanoparticles have different surfaces and atomic arrangements, it was hypothesized that these shapes would result in different catalytic efficiency. It was determined that octahedral and hexapod morphologies produced the greatest amperometric response which proved that the nanoparticle morphology affected its catalytic ability.

Although it is not yet known how to synthesize these particular morphologies on a titania nanotube array, it is known that nanoparticle structure can be manipulated by changing the concentration of the equimolar $CuSO_4/H_2SO_4$ solution during electrode synthesis.[21] By changing the concentration of the $CuSO_4/H_2SO_4$ solution, a variety of heterostructure interface architectures can be synthesized. This Major Qualifying Project works to build of the two-step electrodeposition synthesis of Zhu et al. by relating these varying interface architectures to their glucose sensing capabilities.[26]

Chapter 3: Experimental Theory

3.1 Titanium Pretreatment

It is well established that the biological performance of a material is greatly influenced by its surface properties. Because surface properties are instrumental for medical devices, titanium and other medically relevant materials undergo surface processing. The goal of these processing steps is to establish a well-defined and controllable surface structure. Some important surface processing steps that are employed in the experimental section of this report are described by Brunette et al., and include: polishing, solvent cleaning, pickling, and anodic oxidation.[27, 28]

3.1.1 Polishing

During bulk processing and fabrication methods that recover fresh titanium, the metal is exposed to high temperatures, mechanical stress, and lubricating agents. All of these steps can cause unacceptable deformations and oxidized layers. Polishing titanium metal sheets is performed to remove the native layer of metal and to smooth the surface before further processing. Typically, polishing is performed by using a hard, abrasive medium with successively finer abrasive grades. Mechanical grinding and polishing will lead to plastic deformations and stresses on the surface, but these processing steps are generally used as an intermediate step prior to chemical or electrochemical treatments.

3.1.2 Solvent cleaning

Solvent cleaning is performed to remove oils, greases, and fatty surface contaminants that are left over from the manufacturing of titanium. Common solvents that are used to degrease the titanium surface include aliphatic hydrocarbons, alcohols, ketones, or chlorinated hydrocarbons. The process of solvent cleaning can be carried out in elevated temperatures or in an ultrasonic cleaner. This process is not intended to affect the underlying oxide layer or the surface structure, but most cleaning agents will leave residuals.

3.1.3 Pickling

Pickling, otherwise known as acid etching, is a process used to remove the oxide scales on the metal surface to produce a clean and uniform finish. The most common solution for pickling

consists of 10-30 vol% nitric acid (HNO_3), 1-3 vol% hydrofluoric acid (HF), and DI H_2O. The hydrofluoric acid performs the main function by reacting with the TiO_2 layer and dissolves the titanium. The ratio of HNO_3 to HF should be maintained at 10:1 to minimize embrittlement of the surface layer. This process is typically performed at room temperature for 1-60 minutes where agitation can be used to reduce uneven etching caused by gas bubbles. The topology of the acid etched titanium surfaces maintains the microstructures of the original foil but will generally have a surface oxide layer of less than 10 nm. The surface oxide layer will continue to grow back over time at a rate of 3-6 nm over a 400 day period.

3.2 Electrochemical Techniques

3.2.1 Anodic Oxidation

Anodic oxidation is a form of electrochemical treatment that is often used to modify the surface of metallic specimens via chemical reaction. To perform anodic oxidation, an electrochemical circuit is set up in an electrolyte solution where the metal foil is made the anode. A constant supplied voltage is supplied and current flows through the circuit to promote reactions at both the cathode and anode. In addition to producing nanotubes, the process oxidizes the exposed layers of titanium to form titania or TiO_2. The titania layer provides a protective layer for the nanotubes and is relatively inert. A picture of the experimental setup can be seen in Figure 7 below.

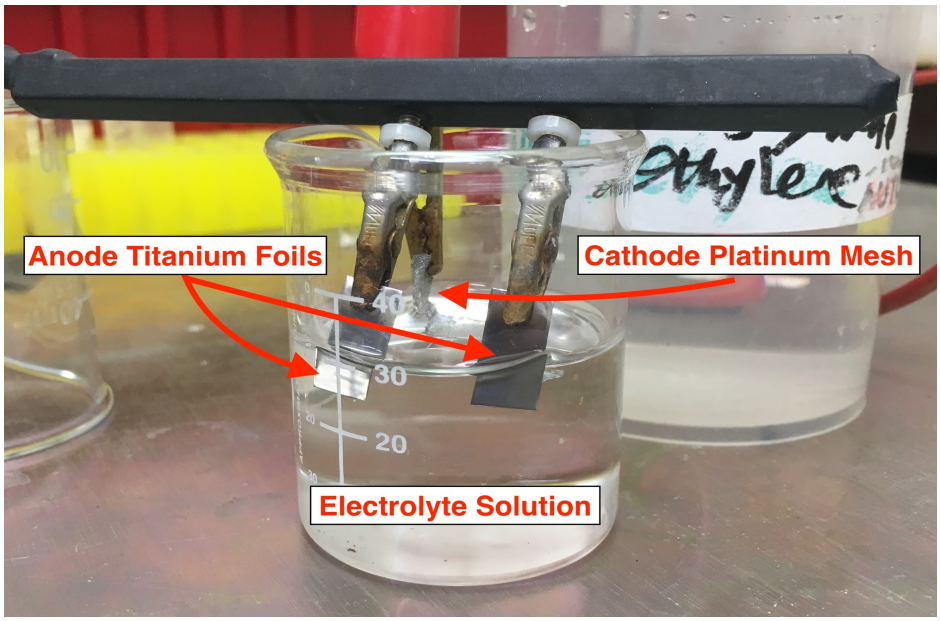

Figure 7: Experimental setup for anodic oxidation.

3.2.2 Three-electrode Setup

A three-electrode technique consisting of a working electrode, counter electrode, and reference electrode. The working electrode is the electrode of interest where a chemical reaction is being monitored. The electrons generated from the chemical reaction are transferred from the working electrode to the counter electrode. This movement of electrodes is measured by an amperometer and the resulting current that results from a set potential is recorded. The reference electrode does not connect to either the working or counter electrode but is used to provide precise control of the working electrode. Figure 8 below shows an experimental set up with the titanium foil as the working electrode, a silver wire as the counter electrode, and an Ag/AgCl probe as the reference electrode.

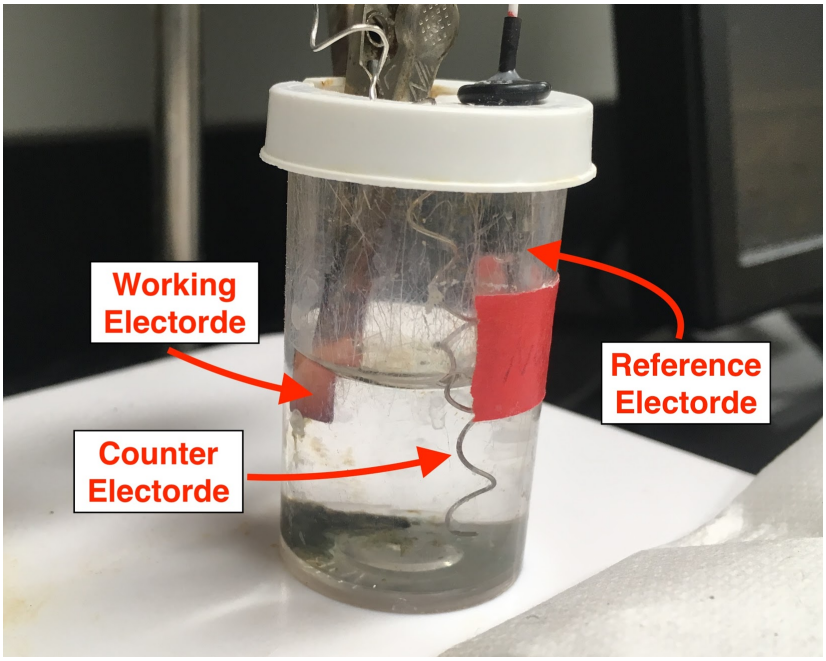

Figure 8: Experimental setup depicting three-electrode cell.

3.2.3 Chronoamperometry

Chronoamperometry is a three-electrode, voltammetric method where the electrochemical potential applied is set and the resulting current is measured. In chronoamperometry the applied voltage increases stepwise from a resting potential to the set potential at time zero. The current jumps to a maximum value and decreases as time goes on due to the diffusion limitations of the reacting species. Figure 9 below depict the applied waveform and Figure 10 shows the resulting voltammogram of this method.

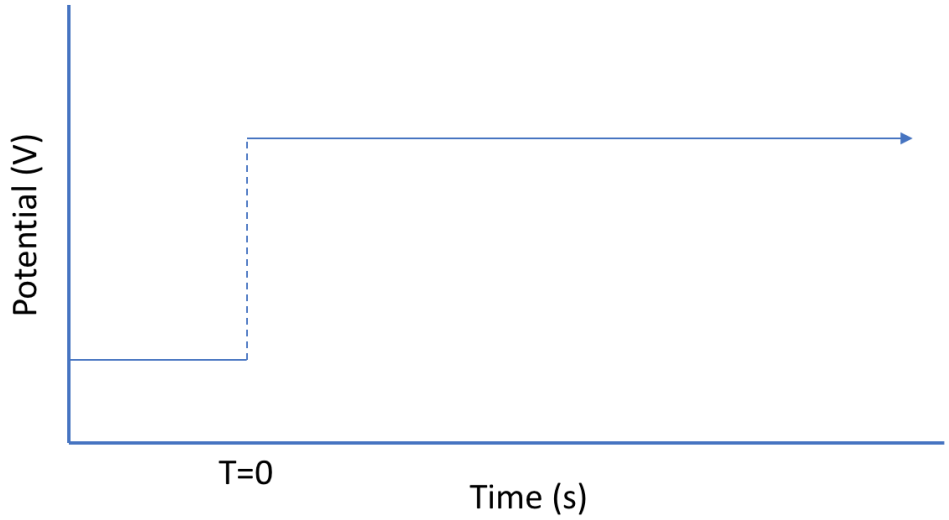

Figure 9: Applied waveform for chronoamperometry.

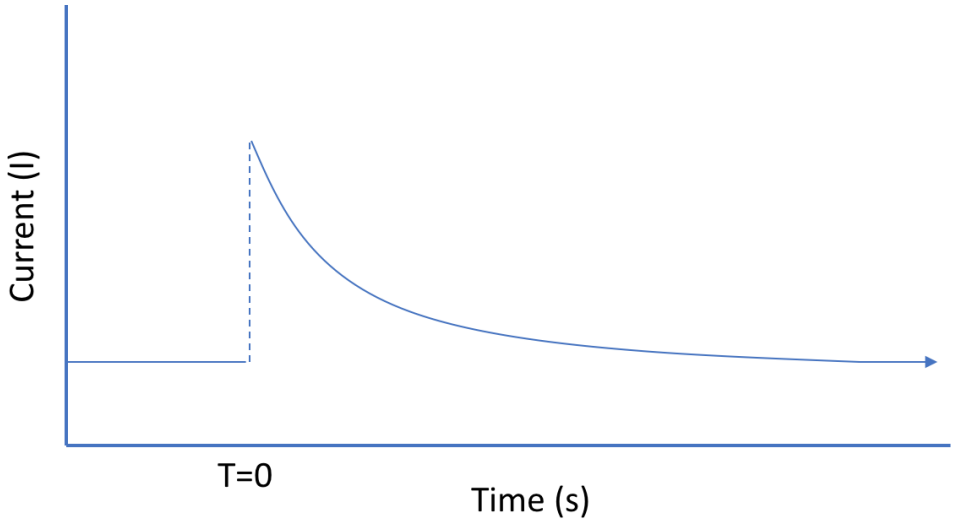

Figure 10: Typical voltammogram for chronoamperometry.

3.2.4 Cyclic Voltammetry

Cyclic voltammetry is another voltammetric technique that requires a three-electrode cell setup. Cyclic voltammetry is a sweeping voltammetric method where two potential peaks are chosen, and the resulting current is monitored. Figure 11 and 12 below depict the applied waveform and resulting voltammogram of this method. In this figure it can be seen that the applied potential to the system cycles between the first and second peak to produce a voltammogram with two peaks. These peaks represent the reductive and oxidative potentials required to push the species of interest in the electrolyte solution to react. The locations and intensities of these peaks can reveal information about the reacting species identity and concentration.

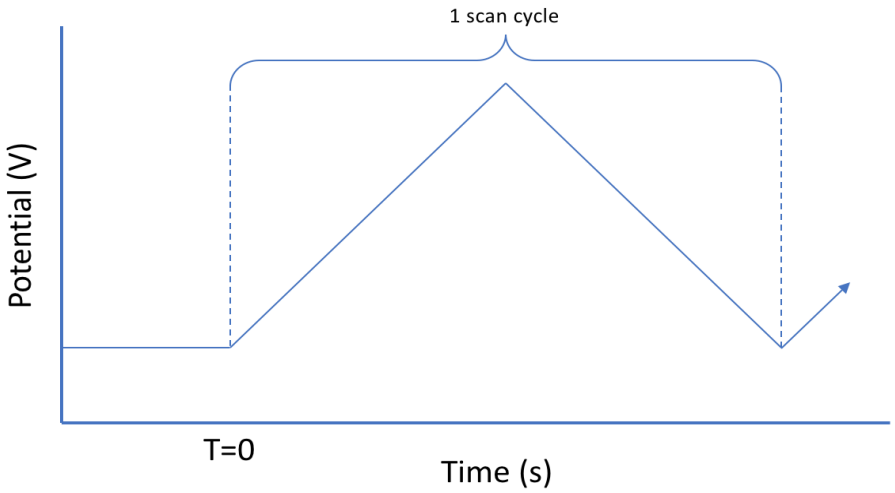

Figure 11: Applied waveform for cyclic voltammetry.

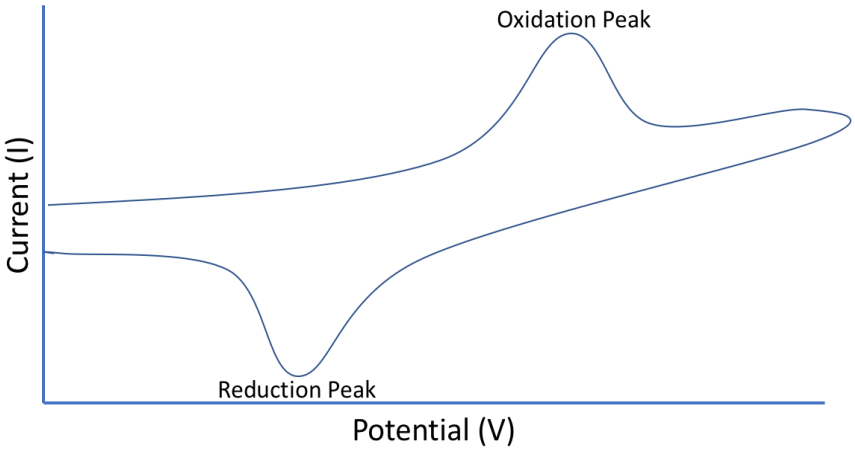

Figure 12: Typical voltammogram for a reversible reaction.

For perfectly reversible systems, certain characteristics of a voltammogram can be identified. In a reversible system, the positions of the anodic and cathodic peak positions do not change with scan rate and the absolute value ratio of the peak currents equal one. Additionally, the peak currents are a function of square root of the scan rate.

3.3 Analytical Techniques

3.3.1 Scanning Electron Microscopy

Scanning electron microscopy (SEM) is an imaging technique that uses a high energy electron beam to produce high resolution images. These images result from the electron-sample interaction which is capable of revealing information such as surface morphology, chemical composition, and crystalline structure. The images were analyzed using the software ImageJ to estimate nanostructure diameters. Figure 13 below shows a sample SEM image.

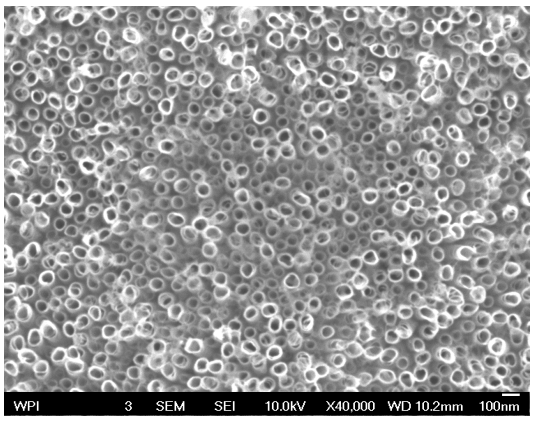

Figure 13: Sample SEM image of titanium nanotube array.

3.3.2 X-ray Diffraction

X-ray diffraction (XRD) is an analytical technique used to identify crystals and crystalline structures. This technology works by firing a beam of electrons at a target that causes electrons in the target to fall from higher valence shells to lower valence shells. When the electrons fall from higher shells to lower, x-rays are emitted. XRD can be performed in an automated x-ray diffractometer and will produce diffraction patterns for the intended specimen. The unique diffraction patterns can be compared to catalogued JCPDS files to assist in phase identification.

Chapter 4: Experimental Setup

4.1 Preparation of TiO_2 Nanotube Array

A titanium sheet (99.7%, Aldrich) was cut into a rectangle (2.5 cm x 1.25 cm) and polished manually using sandpaper for 5 minutes on each side. The foil was then sequentially sonicated in methanol, acetone, ethanol, then DI water for 15 minutes each. Once cleaned, the foil was pickled in an acid solution containing DI water, 70% HNO_3, and 50% HF in a 1:3:1 ratio by volume for approximately a minute. The foil was then rinsed with DI water and connected to the anode of a two-electrode electrochemical cell connected to a direct current (DC) power supply station (DCS80-13E, Sorensen). The electrolyte in the electrochemical cell contained 1 wt% NH_4F dissolved in a 10% vol water in ethylene glycol solution. A platinum mesh was connected to the cathode and the anodic oxidation was run for 45 minutes at 28.5 V. Following anodic oxidation, the foil was annealed at 350°C for 90 minutes then cooled naturally to room temperature overnight.

4.2 Preparation of the CuO/TNT Heterostructure

The prepared titanium nanotube (TNT) array was sonicated in DI water for 15 minutes. Following sonication, the foil was connected to the working electrode in a three-electrode electrochemical setup. The reference electrode was a Ag/AgCl standard and the counter electrode was connected to a platinum wire. The copper nanoparticles were deposited in a two-step electrodeposition method. First, the TNT array was subjected -0.37 V during chronoamperometry for 100 seconds in a solution made up of varying equimolar concentrations of $CuSO_4$+ H_2SO_4 (500 mM, 250 mM, 125 mM, 62.5 mM, 31.3 mM, 15.6 mM, and 7.8 mM). Then, the electrode was scanned in 0.1 M NaOH using cyclic voltammetry (CV) under a potential range of -0.5 V to 0.3 V at 100 $mV \cdot s^{-1}$ for 10 cycles.

4.3 Measurements

Scanning electron microscopy (SEM) was operated at 10 kV using SEM, JEOL, JSM-7000F. The x-ray diffraction (XRD) patterns were generated using Bruker-AXS D8 focus, 40 kV, 40 mm, CuKa radiation. All electrochemical measurements were carried out in an Autolab PGSTAT12 electrochemical workstation (Metrohm, USA Inc.).

Chapter 5: Results and Discussion

5.1 Synthesizing CuO/TNT Heterostructure by Varying Electrolyte Concentration

The titanium nanotubes were synthesized on the foils by polishing, sonicating, acid etching, and anodic oxidation. The resulting foils can be seen below in Figure 14. A line could be clearly seen where the clamp held the foil above the electrolyte solution during the nanotube formation. Thus, nanotubes were only present in the larger of the two divisions. This division was noted, and it was ensured that the clamps would be positioned on the right end during any following electrochemical techniques.

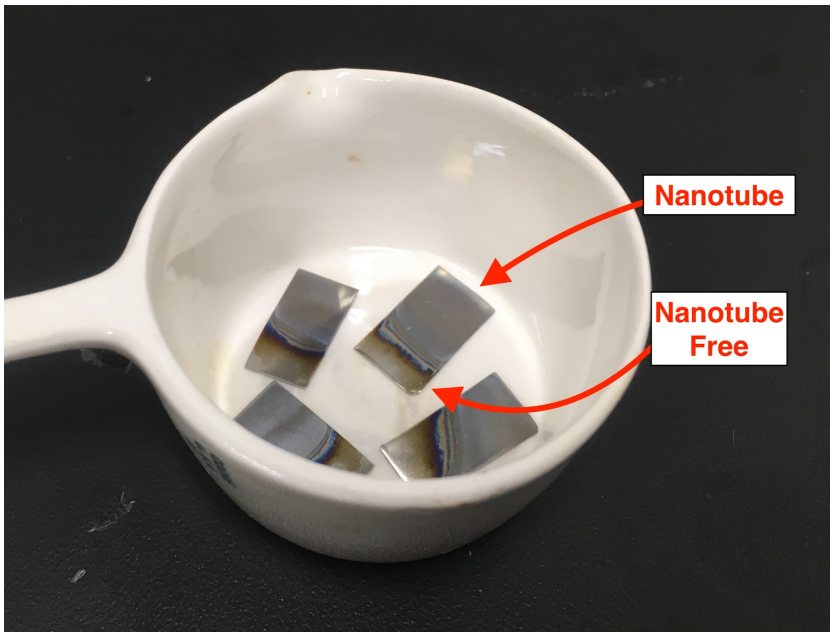

Figure 14: Titanium foils after anodic oxidation.

After the titanium nanotubes were synthesized, the foils were annealed to ensure proper crystal structure. Once the annealing process was complete, many foils seemed to develop a white layer on one side. This layer can be seen in Figure 15 below on the middle foil. It is likely that this layer was due to organic molecules from the air that oxidized and deposited onto the foils. To reduce some of the active site poisoning effects these layers might have on the sensor, the foils were sonicated for 15 minutes in DI water before the copper oxide deposition.

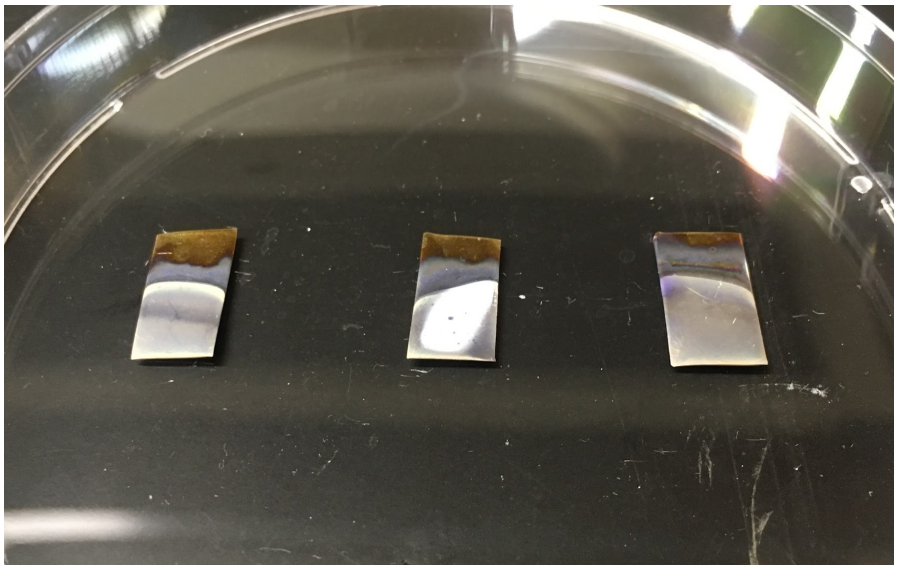

Figure 15: Oxidized layers formed on the foils after annealing.

Once the samples were properly cleaned and prepped, the foils were decorated with copper oxide nanoparticles via chronoamperometry followed by cyclic voltammetry. It was visibly apparent that copper had been deposited onto the nanotubes from the change in color that can be seen in Figure 16 below. As the $CuSO_4$ concentration in the electrolyte decreased, the red covering darkened to a black appearance. The foils produced from the successive dilutions of the $CuSO_4$ can be see below in Figure 17.

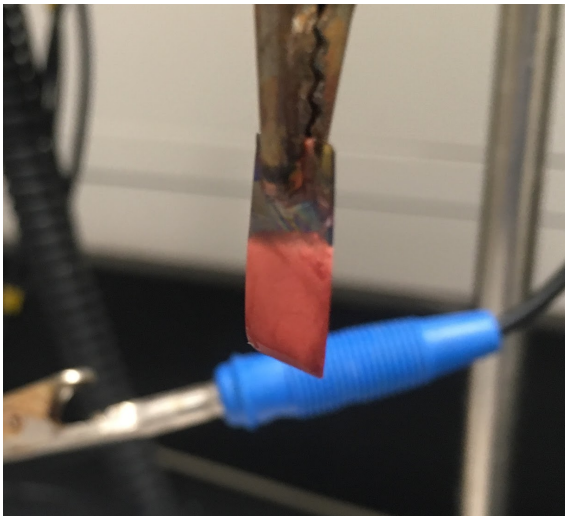

Figure 16: Copper deposition seen on the titanium foil after chronoamperometry.

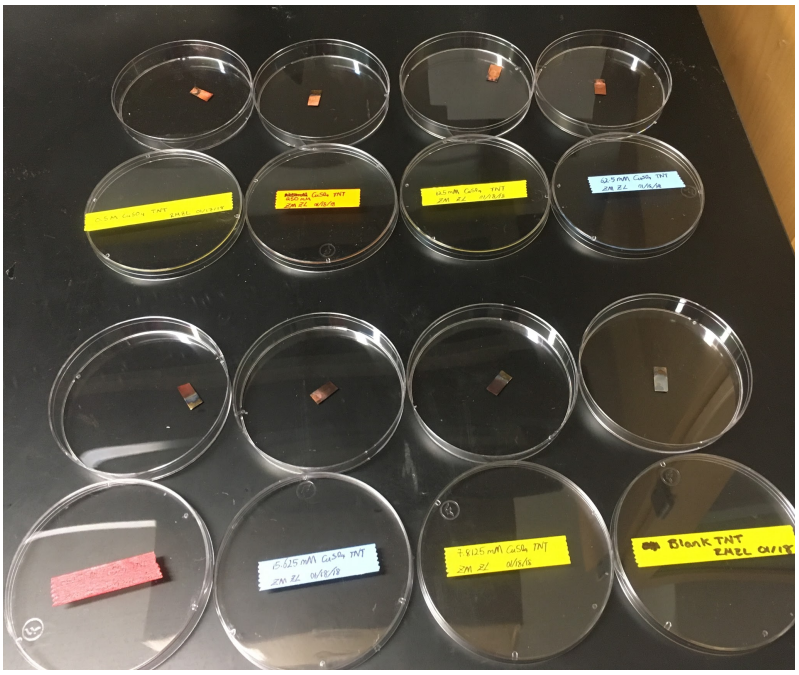

Figure 17: Successive CuSO4 dilutions during chronoamperometry from left to right and top to bottom highlighting color change.

5.2 Investigating a Broad Electrolyte Concentration Range on Electrode Morphology

The CuO/TNT heterostructures were imaged by SEM to analyze the effects of the $CuSO_4$ concentration on electrode morphology. From Figure 18 below, it is apparent that when the concentration of the electrolyte solution increased, the density of copper particles deposited onto the nanotubes also increased. From 7.8 mM to 31.3 mM electrolyte solution, the nanotubes can still be seen between the clusters of copper oxide particles. At concentrations greater than 62.5 mM, however, the nanotubes were almost entirely covered. It is also interesting to note that when the electrolyte concentration exceeded 62.5 mM, nanofibers began to appear. These nanofibers seem to connect the clusters of nanoparticles and may help increase surface area. From the SEM images of the electrodes, the morphology of the electrode surface seemed to shift from sparsely to densely coated with copper between the 31.3 mM and 62.5 mM electrolyte depositions. For simplicity, an electrode synthesized below this shift will be considered low concentration while an electrode synthesized above this shift will be considered high concentration. Figure 19 below highlights the copper oxide clusters and nanofibers imaged on the 62.5 mM electrode.

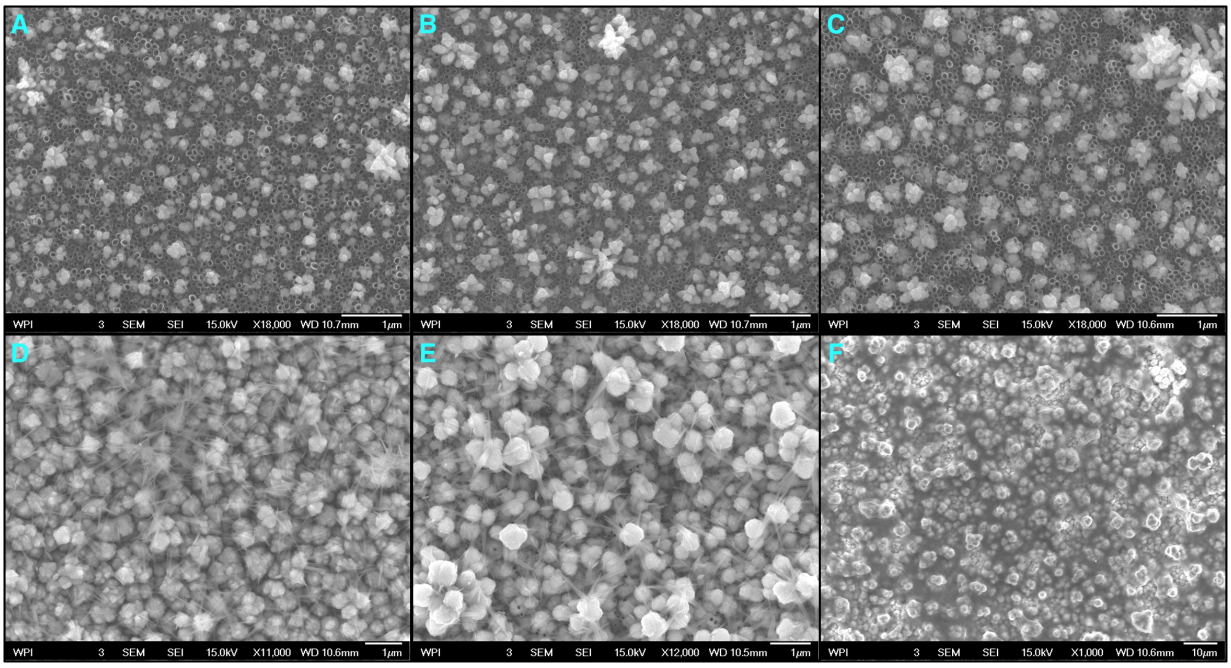

Figure 18: SEM imaging of Cu2O/TNT heterostructures developed using chronoamperometry in an electrolyte solution of CuSO4 and H2SO4 at concentrations of (a) 7.8 mM; (b) 15.6 mM; (c) 31.2 mM; (d) 62.5 mM; (e) 125 mM; and (f) 250 mM.

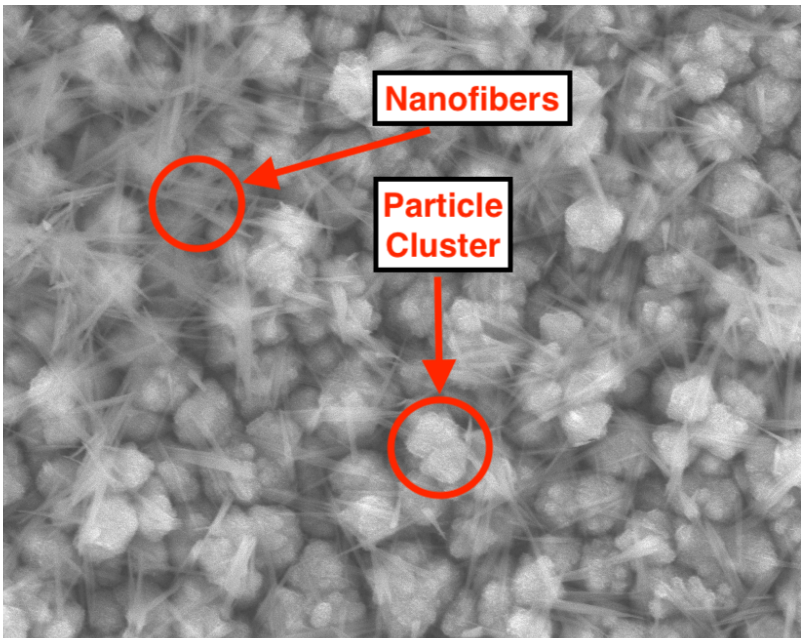

Figure 19: SEM image of the 62.5 mM Cu2O/TNT heterostructure highlighting nanofibers and copper oxide nanoparticle cluster.

The software ImageJ was used to calculate the average size of the nanoparticles and the diameters were graphed in Figure 20 below as a function of $CuSO_4/H_2SO_4$ concentration. At the low concentrations of 7.8 mM, 15.6 mM, and 31.3 mM, the diameters of the nanoparticles were measured to be 280 ± 40 nm, 365 ± 60 nm, and 400 ± 90 nm respectively. The nanotube diameter, however, was measured to be about 90 ± 10 nm. Due to the size difference between the clusters and the nanotubes, it is unlikely that the copper is able to coat the scaffold and take full advantage of the entire surface area. The cluster sizes continued to increase with increasing electrolyte concentration and the measured values for the 62.5 mM, 125 mM, and 250 mM electrodes were 620 ± 140 nm, 720 ± 120 nm, and 5200 ± 1800 nm respectively. This trend clearly shows that increasing the electrolyte solution concentration also increased the size of the nanoparticles deposited on the surface of the nanotube array.

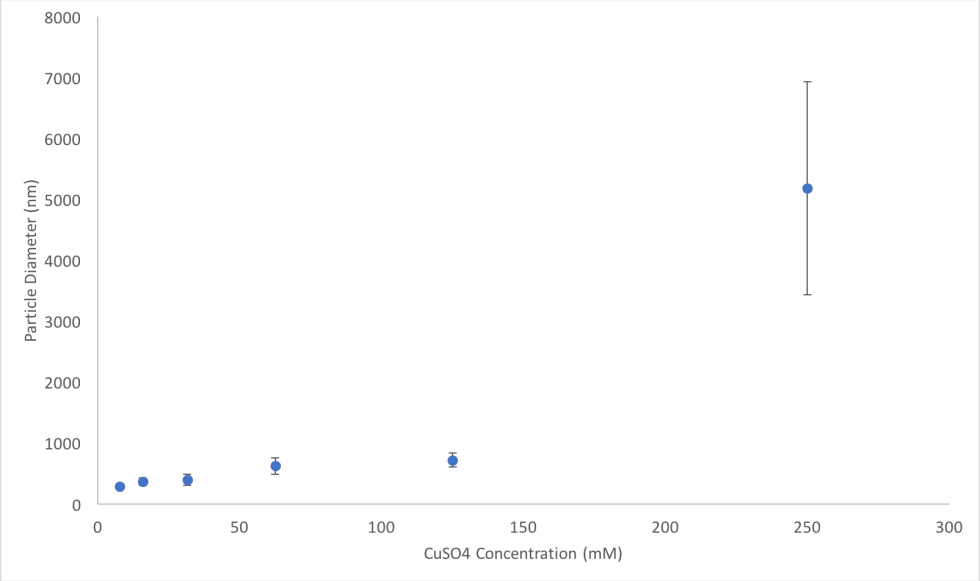

Figure 20: ImageJ measurements of the nanoparticle diameters as a function of the CuSO4/H2SO4 concentration.

5.3 Investigating a Broad Electrolyte Concentration Range on Electrode Function

The cyclic voltammograms for all of the electrodes synthesized under chronoamperometry in equimolar $CuSO_4 + H_2SO_4$ solutions can be seen in Appendix A. Figure 21 below shows the cyclic voltammogram produced for a low concentration electrode (15 mM) and for the bare titanium nanotube electrode in a glucose and glucose free electrolyte solution. None of the low concentration electrodes or blank electrode showed an obvious oxidation or reduction peak.

Because these electrodes lack clear oxidation peaks, it is likely that the electrodes were not effectively catalyzing the oxidation of glucose. The low concentration electrodes and the blank electrode, however, significantly increased in current when scanned in a glucose solution compared to a glucose free solution. The peak currents in the glucose solution were over 30 times greater than the current in the glucose free solution. In general, the low concentration electrodes function with similar ability to the blank and there is no clear advantage for the copper deposition step at these concentrations.

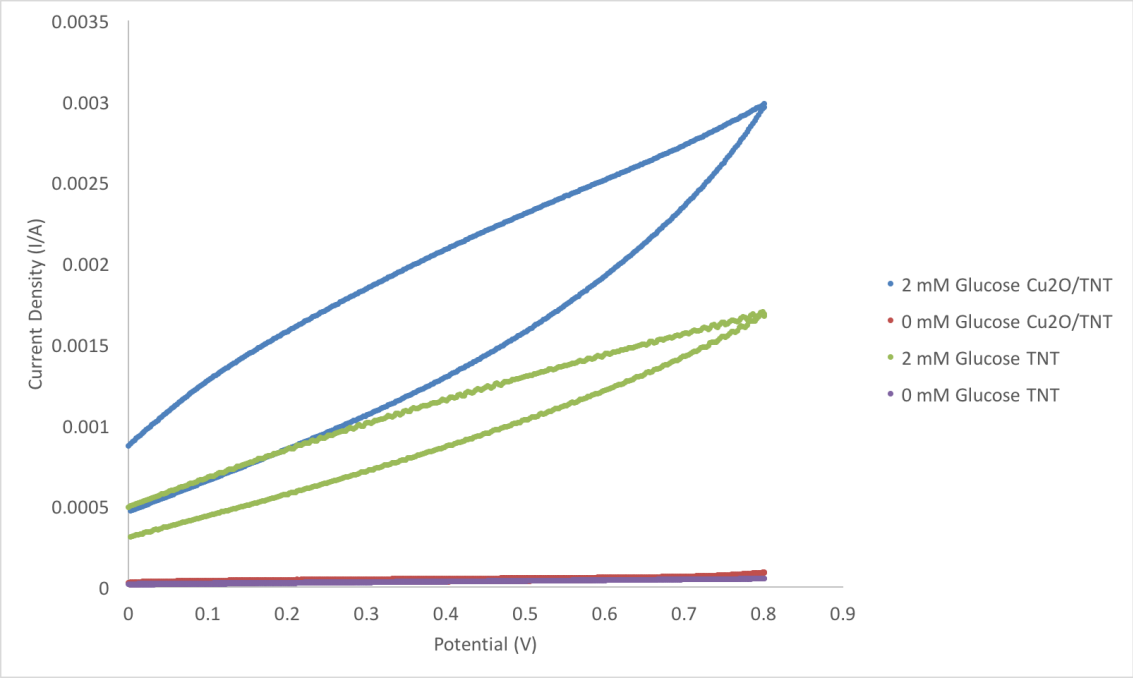

Figure 21: Cyclic voltammogram for 15.6 mM electrode in 0.1 M NaOH + 2 mM glucose (blue) and in 0.1 M NaOH (red). Cyclic voltammogram for bare titanium nanotube array in 0.1 M NaOH + 2 mM glucose (green) and in 0.1 M NaOH (purple).

Figure 22 below shows the cyclic voltammogram for a high concentration electrode (125 mM) and for the bare titanium nanotube electrode in a glucose and glucose free electrolyte solution. The high concentration electrodes exhibited oxidation peaks at approximately 0.55 V. Because there were oxidation peaks, it can be confirmed that the electrodes were effectively catalyzing the oxidation of glucose. All electrodes showed an increase in peak current density when scanned in the glucose containing electrolyte versus the glucose free electrolyte. The high concentration electrodes, however, only showed minor peak current increases. For example, the peak current

increased by 1.4 times in a glucose solution when compared to a glucose free solution for the 125 mM electrode. This low current increased for the high concentration electrodes suggests that the electrodes were no longer selectively oxidizing glucose. Because glucose oxidation is kinetically controlled, and kinetic limitations can be overcome by increasing surface area, it is probable that the high surface area provided by the titanium nanotube array is no longer advantageous. The SEM images support this estimate because the copper oxide nanoparticles appear to completely coat the nanotube array. Although the high concentration electrodes seemed to not selectively oxidize glucose, they did produce peak currents that were much greater than the blank. These high concentration electrodes all exhibited similar functions of high current due to dense copper composition but low current improvement in the glucose containing solution due to a decrease in effective surface area.

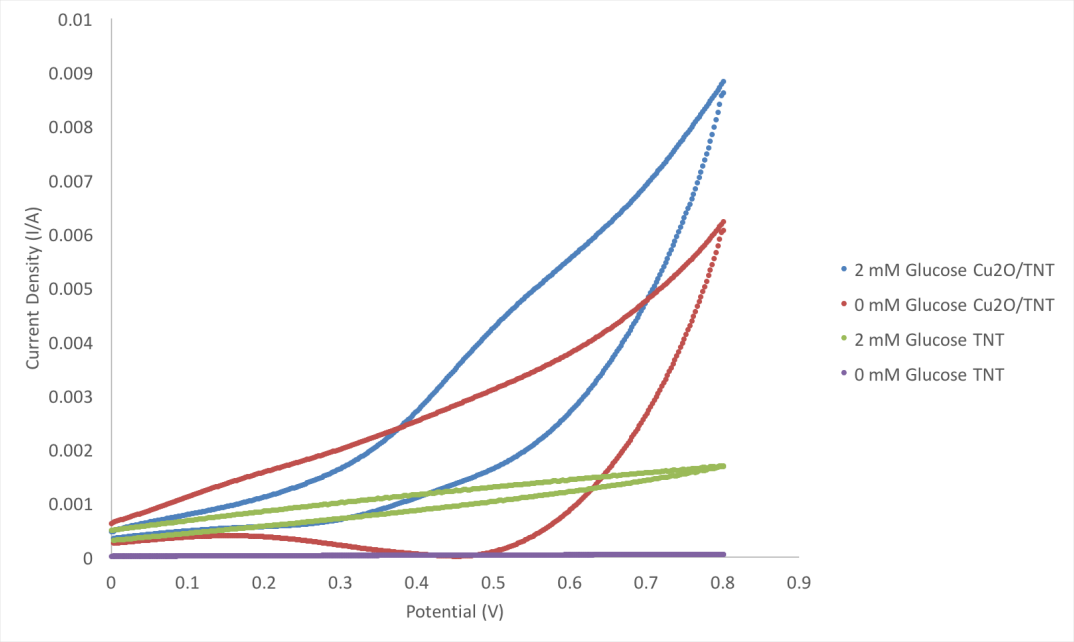

Figure 22: Cyclic voltammogram for 125 mM electrode in 0.1 M NaOH + 2 mM glucose (blue) and in 0.1 M NaOH (red). Cyclic voltammogram for bare titanium nanotube array in 0.1 M NaOH + 2 mM glucose (green) and in 0.1 M NaOH (purple).

Because the 62.5 mM synthesized electrode produced the most defined oxidation peak, a chronoamperometric experiment was conducted to better understand the linear range for glucose sensing. This response curve, seen in Figure 23 below, took place in 0.1 M NaOH with the addition of successive 0.2 M glucose samples. The sensor electrode exhibits linearity for glucose sensing

in a range from 0.2 to 0.8 mM. From Figure 24, it can be seen that there is a correlation coefficient of 0.962 in this range with a sensitivity calculated from the slope to be 686 $uA \cdot mM^{-1} \cdot SA^{-1}$. This sensor has a limited linear sensitivity range for glucose sensing which would not be appropriate for blood samples that contain glucose at concentrations ~ 4mM.

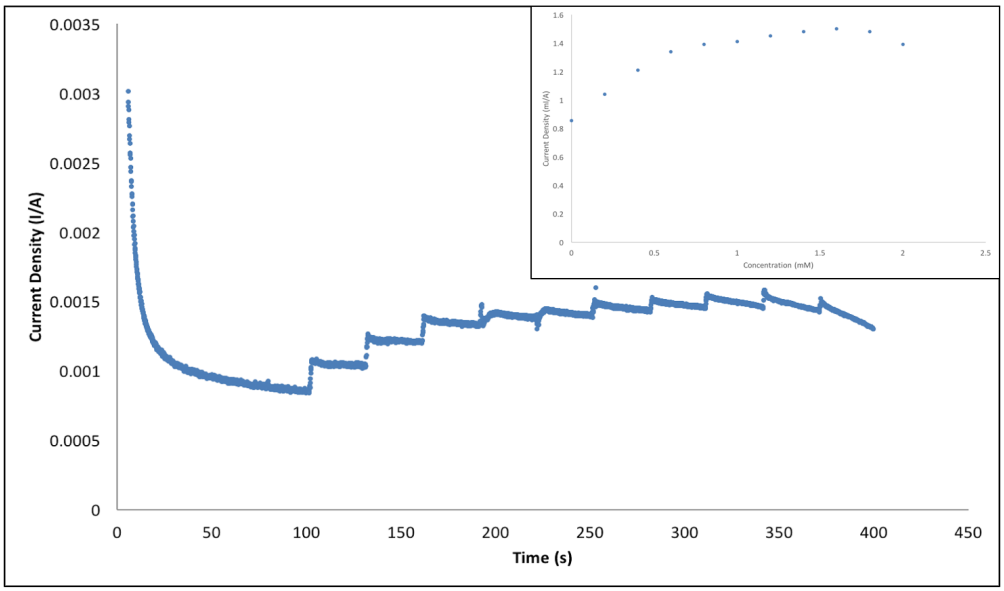

Figure 23: Amperometric measurement of CuO/TNT electrode developed by chronoamperometry with 62.5 mM CuSO4. Response with successive additions of 0.2 mM glucose in 0.10 M NaOH. Inlet is the calibration curve of current response versus glucose concentration.

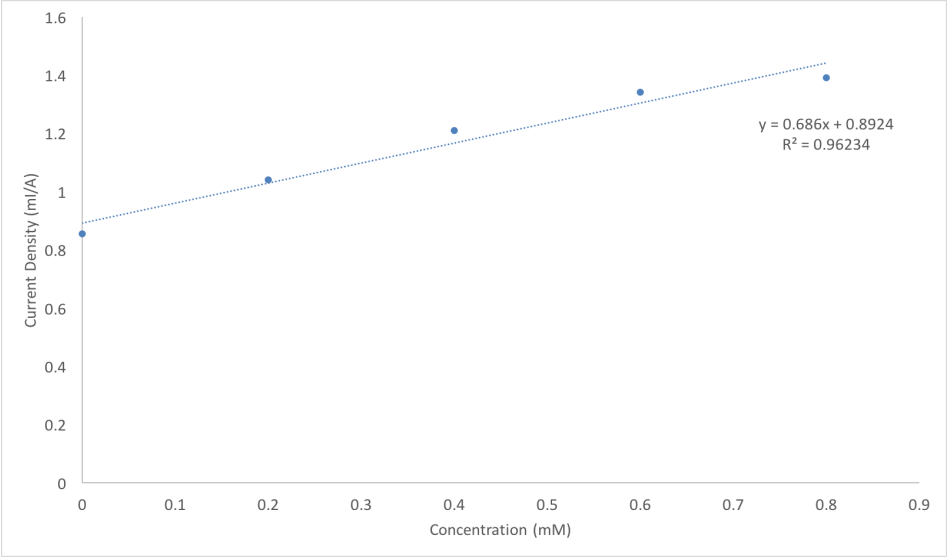

Figure 24: Linear glucose sensing range for CuO/TNT electrode synthesized by chronoamperometry with 62.5 mM CuSO4.

From the synthesis of the electrodes in the equimolar $CuSO_4$ + H_2SO_4 electrolyte solution using chronoamperometry it seems that the titanium nanotube array provided a high surface area that is beneficial for selective glucose sensing while the copper oxide increased the measureable current amplitude. It would be most ideal to produce an electrode that has both high sensitivity for glucose and high current density reading. From the SEM images and cyclic voltammograms there seemed to be a transition from low copper oxide density to high copper oxide density between the 31.3 mM and 62.5 mM synthesized electrodes. To better investigate this concentration range, four more electrodes were synthesized in 30, 40, 50, and 60 mM $CuSO_4/H_2SO_4$ and analyzed by cyclic voltammetry and chronoamperometry.

5.4 Investigating a Narrow $CuSO_4/H_2SO_4$ Concentration Range on Electrode Function

The four narrow ranged electrolyte electrodes were synthesized and scanned by cyclic voltammetry in glucose concentrations that varied from 0 mM to 10 mM. The resulting voltammograms for each electrode can be seen in Appendix B. Figure 25 below shows the scans from the 50 mM electrode with 0 mM being the lightest blue and 10 mM being the darkest blue. From this graph it can be concluded that by increasing the glucose concentration during the cyclic voltammetry scans the resulting current reading also increased. The increase in current can be attributed to the increase in availability of glucose for catalysis.

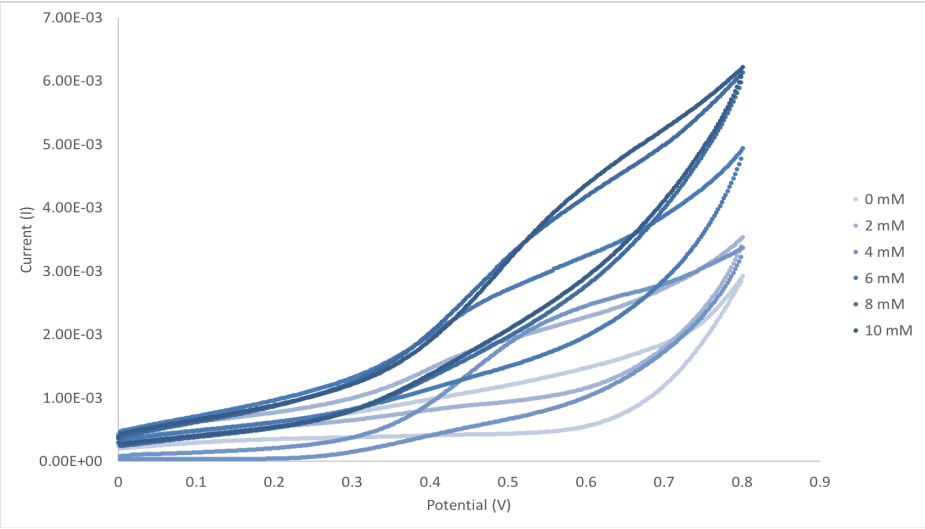

Figure 25: Cyclic voltammograms of 50 mM synthesized electrode in 0 mM (light) to 10 mM (dark) glucose solutions.

In addition to analyzing glucose concentration on current readings, the four narrow ranged electrodes were compared to one another by cyclic voltammetry. In general, at each concentration of glucose, the current reading was lowest for the 30 mM electrode and increased in response to the increasing deposition concentration. This current increase as a response to increasing $CuSO_4$ concentration during copper deposition is demonstrated below in Figure 26. This trend is likely due to an increase in copper oxide density on the electrode surface as a response to electrolyte concentration that enhanced the catalysis ability. It was shown in the previous analysis of the broad ranged electrolyte syntheses that increasing the $CuSO_4/H_2SO_4$ concentration during copper deposition increased the copper density on the electrode surface. Interestingly, the 50 mM electrode depicted by the green cycle in Figure 26 exhibits the most prominent oxidation peak. The 50 mM electrode maintained the most well-defined cyclic voltammogram across all glucose scan ranges.

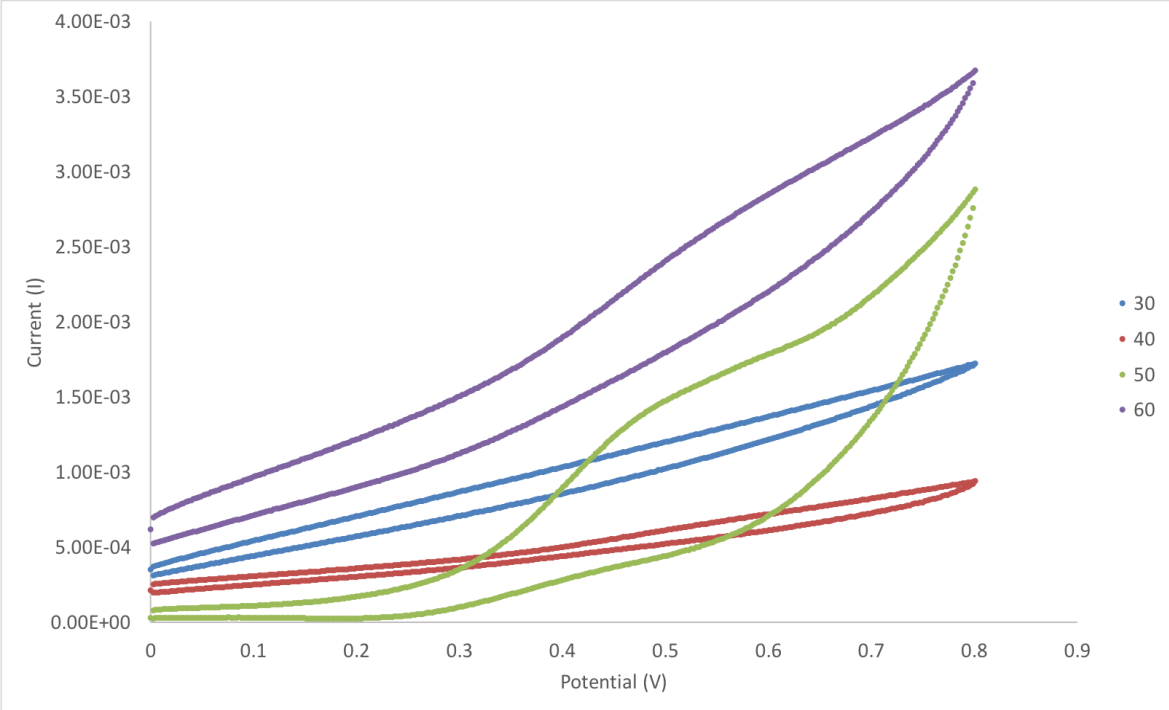

Figure 26: Cyclic voltammograms of 30 mM (blue), 40 mM (red), 50 mM (green), and 60 mM (purple) synthesized electrodes in a 4 mM glucose solution.

Because the 50 mM and 60 mM synthesized electrodes produced the most defined oxidation peaks, a chronoamperometric experiment was conducted to better understand the linear range for glucose sensing. The response curves, seen in Figure 27 below, took place in 0.1 M NaOH with the addition of successive 0.2 M glucose samples. The sensor electrode exhibits linearity for glucose sensing in a range from 0.2 to 0.6 mM for the 50 mM electrode while the 60 mM electrode exhibits no linearity. From Figure 27, it can be seen that there is a correlation coefficient of 0.919 in this range with a sensitivity calculated from the slope to be 1021 $uA \cdot mM^{-1} \cdot SA^{-1}$. Although better than the 60 mM sensor, the 50 mM sensor has a limited linear sensitivity range for glucose sensing which would not be appropriate for blood samples that contain glucose at concentrations ~ 4mM.

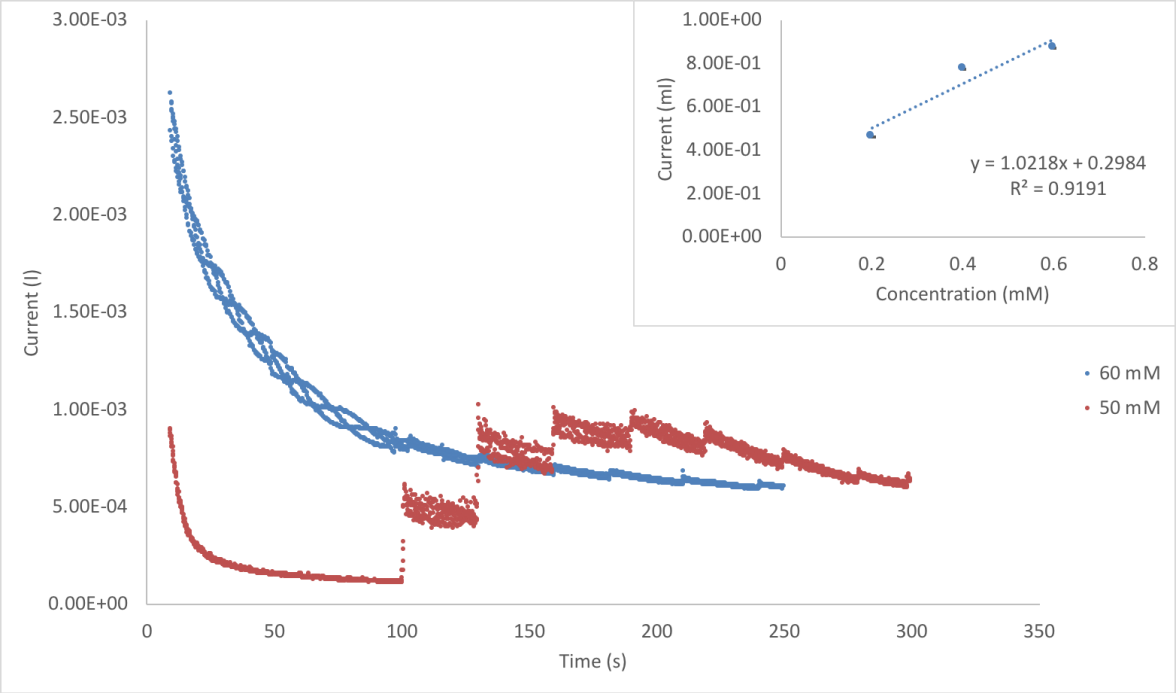

Figure 27: Amperometric measurement of Cu2O/TNT electrode developed by chronoamperometry with 60 mM CuSO4 (blue) and 50 mM CuSO4 (red). Response with successive additions of 0.2 mM glucose in 0.10 M NaOH. Inlet is the calibration curve of current response versus concentration glucose.

After conducting the cyclic voltammograms and chronoamperometric experiments it was determined that for the current experimental setup, 50 mM is the most optimal concentration for the equimolar $CuSO_4/H_2SO_4$ solution. The resulting electrode maintained the most prominent peaks during the cyclic voltammetry scans and had the most linear glucose sensing concentration range.

5.5 UV Irradiation Improves Electrode Function

Due to the UV induced amphiphilicity of TiO_2, the 50 mM and 60 mM foils were exposed to UV light for 30 minutes to test the self-cleaning nature of the heterostructures. Figure 28 below depicts the experimental setup for the UV irradiation.

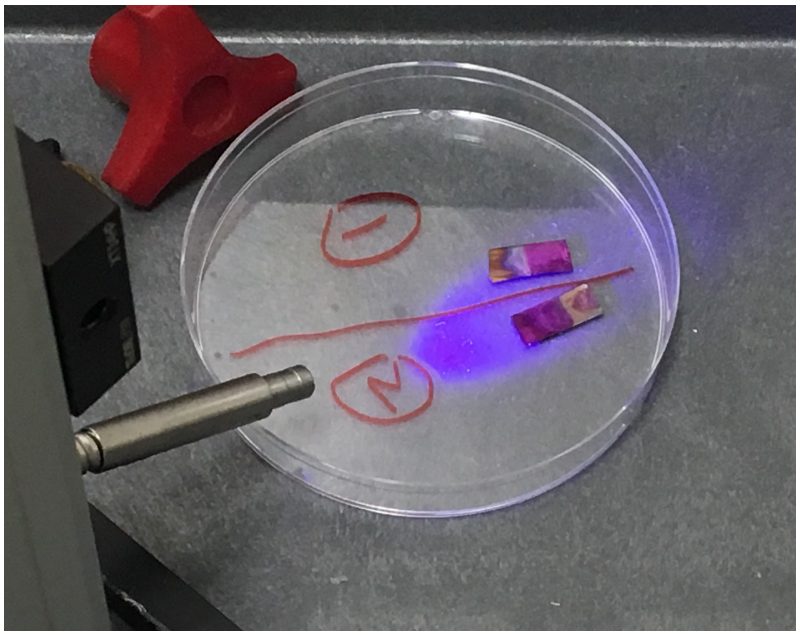

Figure 28: Experimental setup for UV irradiation of CuO/TNT heterostructures.

Following the UV irradiation, the foils were tested for glucose sensitivity by chronoamperometry with 0.2 mM glucose injections and compared to their performance before UV irradiation. Figure 29 below depicts the resulting curves for both foils before and after UV irradiation. It can be seen that both foils decrease in the current amplitude after UV irradiation, but they both exhibit improved glucose sensitivity ranges. Although the 60 mM electrode still does not have a clear linear range, the 50 mM electrode showed a linear sensing range of 0.2 to 1.0 mM glucose. This is an improvement upon the previous experiment done without UV irradiation where the 60 mM electrode had a linear range from 0.2 to 0.6. In addition to a greater range, the linear coefficient improved to 0.964 with a sensitivity calculated from the slope to be 860 $uA \cdot mM^{-1} \cdot SA^{-1}$. Although this electrode is still not sufficient for the great range of glucose found in biofluids, the slight improvement of the linear sensing range does suggest that UV irradiation has some restorative or self-cleaning effect on the heterostructures.

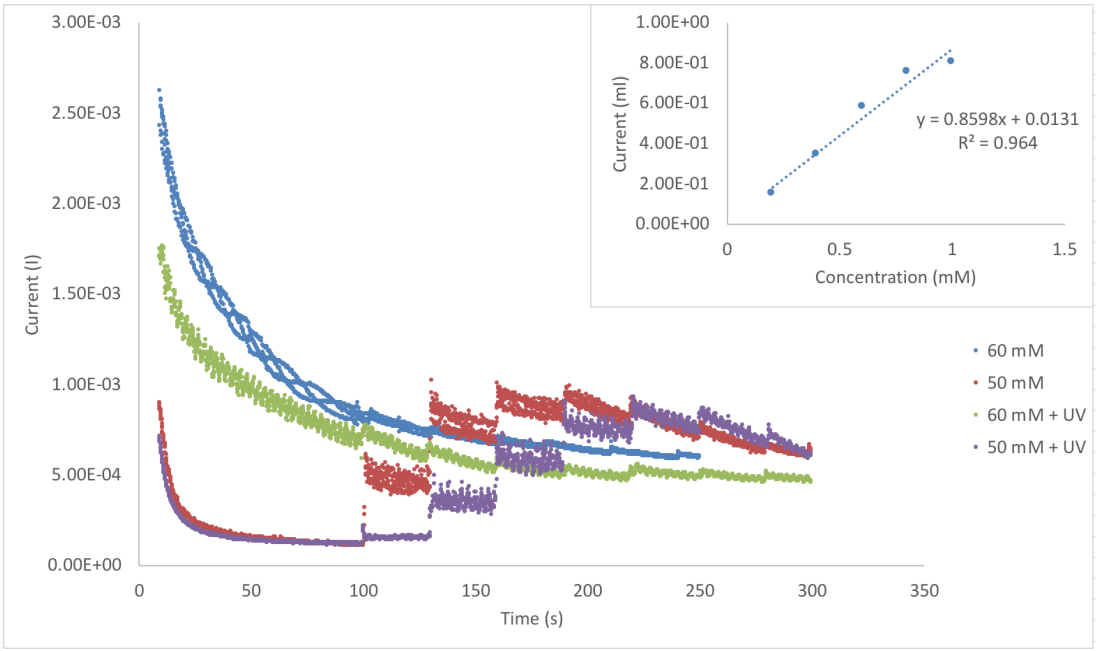

Figure 29: Amperometric measurement of 60 mM electrode before UV (blue) and after UV (green), and 50 mM electrode before UV (red) and after UV (purple). Response with successive additions of 0.2 mM glucose in 0.10 M NaOH. Inlet is calibration curve of current response versus glucose concentration.

The above experiment does show that UV light improved the function of the 50 and 60 mM electrodes, but it cannot prove if original sensing capabilities were recovered. In order to determine the extent to which UV light recovers glucose sensing capabilities, the foils should be immediately tested for glucose sensitivity after they are synthesized. Once glucose sensitivity decreases, the electrodes should be exposed to UV irradiation and then tested for resulting sensitivity. The UV exposed sensitivity can then be compared to its initial sensitivity to determine percent recovery.

5.6 Electrochemical Deposition Techniques Affect Nanoparticle Morphology

In addition to the current method for nanoparticle deposition, square wave voltammetry and other electrochemical methods may be employed to alter nanoparticle morphology. Figure 30 below depicts three electrodes that were synthesized in an electrolyte solution containing 125 mM $CuSO_4/H_2SO_4$. The image in section A is an electrode synthesized via chronoamperometry, while section B and C depict electrodes synthesized via square wave voltammetry. The chronoamperometry method completely saturated the titanium nanotube array with large copper nanoparticles while the square wave voltammetry method produced a less dense layer of copper with a large variety of nanoparticle sizes. This shows that different voltammetry deposition methods produce copper oxide nanoparticles with different morphologies. Further experimentation should be done to determine the best deposition method that produces both a dense covering of copper oxide with a high surface area of small particles.

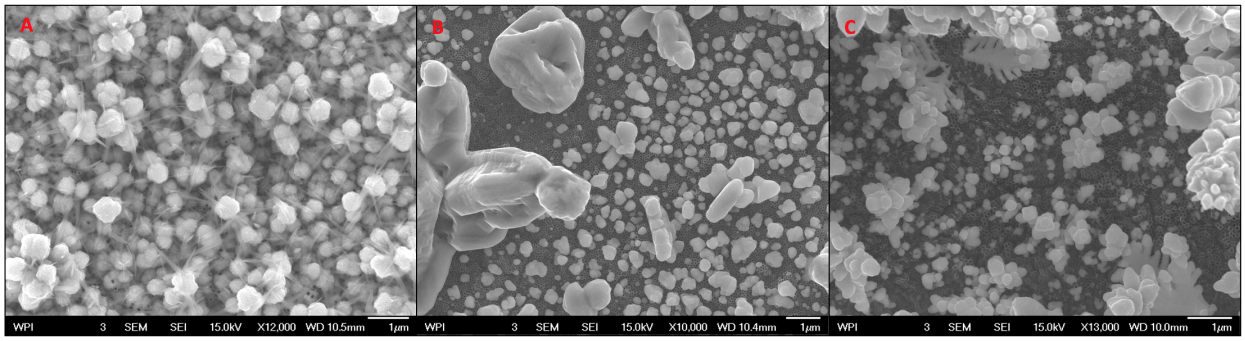

Figure 30: SEM image of electrode synthesized in a 125 mM CuSO4/H2SO4 electrolyte by (a) chronoamperometry, (b) square wave voltammetry with a step potential of 0.005V, (c) square wave voltammetry with a step potential of 0.0024 V.

Chapter 6: Conclusion and Recommendation

This Major Qualifying Project demonstrated that glucose detection capabilities for non-enzymatic electrochemical glucose biosensors can be modified by careful manipulation of the interface architecture. The best sensor was synthesized by the two-step chronoamperometric deposition of copper oxide at 50 mM $CuSO_4/H_2SO_4$. This concentration produced an electrode that exhibited pronounced oxidation peaks during the cyclic voltammetry scans indicating effective catalysis of glucose. In addition to pronounced peaks, this electrode had a linear glucose sensitivity that ranged from 0.2 to 1.0 mM glucose with a correlation coefficient of 0.964. The resulting electrode, however, does not have a sufficient sensing range for industrial applications. Further manipulation of the deposition potential or possibly the deposition method should be explored. It is likely that a different synthesis method which produces copper oxide nanoparticles that coat the inside of the nanotube array will perform with both high amperometric readings and effective glucose selectivity.

References

[1] Newman, Jeffrey D., and Anthony PF Turner. "Home blood glucose biosensors: a commercial perspective." Biosensors and Bioelectronics 20.12 (2005): 2435-2453.

[2] World Health Organization. Global report on diabetes. World Health Organization, 2016.

[3] Li, Zexian, et al. "A Low-Cost and High Sensitive Paper-Based Microfluidic Device for Rapid Detection of Glucose in Fruit." Food Analytical Methods 10.3 (2017): 666-674.

[4] Willems, Jamie L., and Nicholas H. Low. "Authenticity analysis of pear juice employing chromatographic fingerprinting." Journal of agricultural and food chemistry 62.48 (2014): 11737-11747.

[5] Porep, Jan U., et al. "Rapid determination of ergosterol in grape mashes for grape rot indication and further quality assessment by means of an industrial near infrared/visible (NIR/VIS) spectrometer–a feasibility study." Food control 43 (2014): 142-149.

[6] Grieshaber, Dorothee, et al. "Electrochemical biosensors-sensor principles and architectures." Sensors 8.3 (2008): 1400-1458.

[7] Newman, Jeffrey D., and Anthony PF Turner. "Home blood glucose biosensors: a commercial perspective." Biosensors and Bioelectronics 20.12 (2005): 2435-2453.

[8] Ratner, Buddy D. "A perspective on titanium biocompatibility." Titanium in medicine. Springer, Berlin, Heidelberg, 2001. 1-12.

[9] Macak, Jan M., et al. "TiO2 nanotubes: Self-organized electrochemical formation, properties and applications." Current Opinion in Solid State and Materials Science 11.1-2 (2007): 3-18.

[10] Beden, B., et al. "Fourier transform infrared reflectance spectroscopic investigation of the electrocatalytic oxidation of D-glucose: identification of reactive intermediates and reaction products." Electrochimica Acta 41.5 (1996): 701-709.

[11] Fogler, H. S. (2016). *Elements of chemical reaction engineering*. Harlow: Pearson Education.

[12] Song, Yan-Yan, et al. "TiO2 nanotubes: efficient suppression of top etching during anodic growth key to improved high aspect ratio geometries." Electrochemical and Solid-State Letters 12.7 (2009): C17-C20.

[13] Albu, Sergiu P., et al. "Formation of Double-Walled TiO2 Nanotubes and Robust Anatase Membranes." Advanced Materials 20.21 (2008): 4135-4139.

[14] Wang, Rong, et al. "Light-induced amphiphilic surfaces." nature 388 (1997): 431-432.

[15] Macak, Jan M., et al. "Self-Organized TiO2 Nanotube Layers as Highly Efficient Photocatalysts." small 3.2 (2007): 300-304.

[16] Song, Yan-Yan, et al. "TiO2 Nano Test Tubes as a Self-Cleaning Platform for High-Sensitivity Immunoassays." Small 6.11 (2010): 1180-1184.

[17] Park, Sangyun, et al. "Nonenzymatic continuous glucose monitoring in human whole blood using electrified nanoporous Pt." Biosensors and Bioelectronics 31.1 (2012): 284-291.

[18] Wang, Guangfeng, et al. "Non-enzymatic electrochemical sensing of glucose." Microchimica Acta 180.3-4 (2013): 161-186.

[19] Yang, Jing-He, Ketian Zhang, and Ding Ma. "Gourd-shaped silver nanoparticle–graphene composite for electrochemical oxidation of glucose." Materials Letters 97 (2013): 133-136.

[20] Hou, Chuantao, et al. "Metal–organic framework templated synthesis of Co 3 O 4 nanoparticles for direct glucose and H 2 O 2 detection." Analyst 137.24 (2012): 5803-5808.

[21] Huang, Lei, et al. "Controlled synthesis of octahedral Cu2O on TiO2 nanotube arrays by electrochemical deposition." *Materials Chemistry and Physics* 130.1 (2011): 316-322.

[22] Long, Mei, et al. "Novel helical TiO 2 nanotube arrays modified by Cu 2 O for enzyme-free glucose oxidation." Biosensors and Bioelectronics 59 (2014): 243-250.

[23] Qin, Yongqiang, et al. "Supercapacitive performance of electrochemically doped TiO 2 nanotube arrays decorated with Cu 2 O nanoparticles." RSC Advances 6.53 (2016): 47669-47675.

[24] Xiang, Liyun, et al. "Fabrication of Cu2O/TiO2 nanotube arrays with enhanced visible-light photoelectrocatalytic activity." Applied Physics A123.3 (2017): 160.

[25] Won, Yu-Ho, and Lia A. Stanciu. "Cu2O and Au/Cu2O particles: surface properties and applications in glucose sensing." Sensors 12.10 (2012): 13019-13033.

[26] Zhu, Zanzan, et al. “A novel non-enzymatic glucose biosensor based on CuO nanoparticle-decorated TiO_2 nanotube arrays.” Worcester Polytechnic Institute (2016)

[27] Brunette, D. M., et al. "Titanium in medicine: material science, surface science, engineering, biological responses and medical applications (engineering materials)." (2001).

[28] Lausmaa, Jukka. "Mechanical, thermal, chemical and electrochemical surface treatment of titanium." Titanium in medicine. Springer Berlin Heidelberg, 2001. 231-266.

Appendix A: Cyclic Voltammograms for Electrodes Synthesized Under Broad Electrolyte Concentration Range

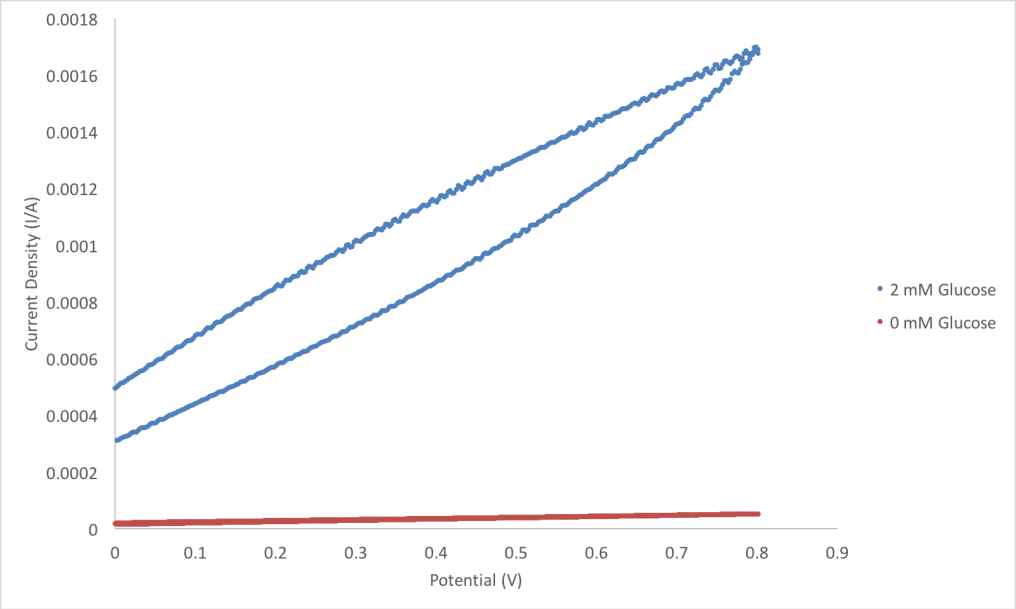

Figure 31: Cyclic voltammogram for blank titanium nanotube array in 2 mM glucose (blue) and in 0 mM glucose (red).

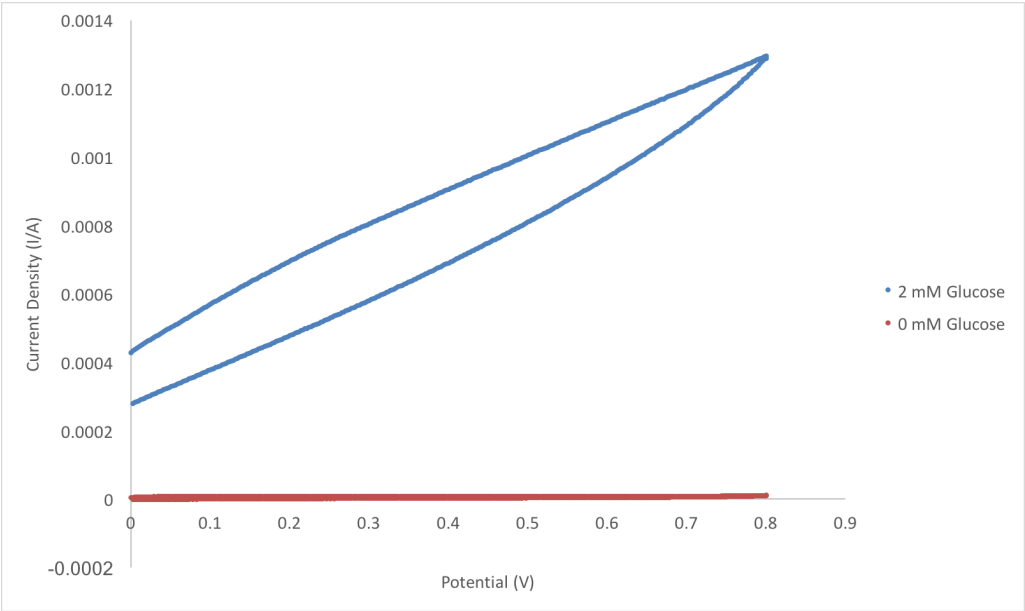

Figure 32: Cyclic voltammogram for 7.8 mM CuSO4 + H2SO4 synthesized electrode in 2 mM glucose (blue) and in 0 mM glucose (red).

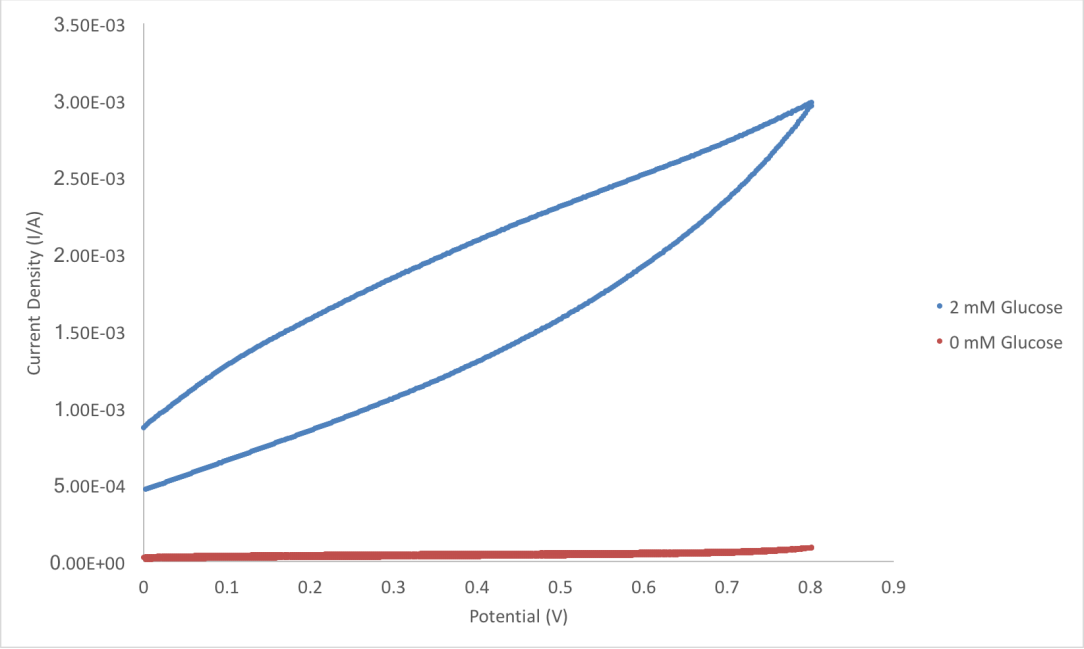

Figure 33: Cyclic voltammogram for 15.6 mM CuSO4 + H2SO4 synthesized electrode in 2 mM glucose (blue) and in 0 mM glucose (red).

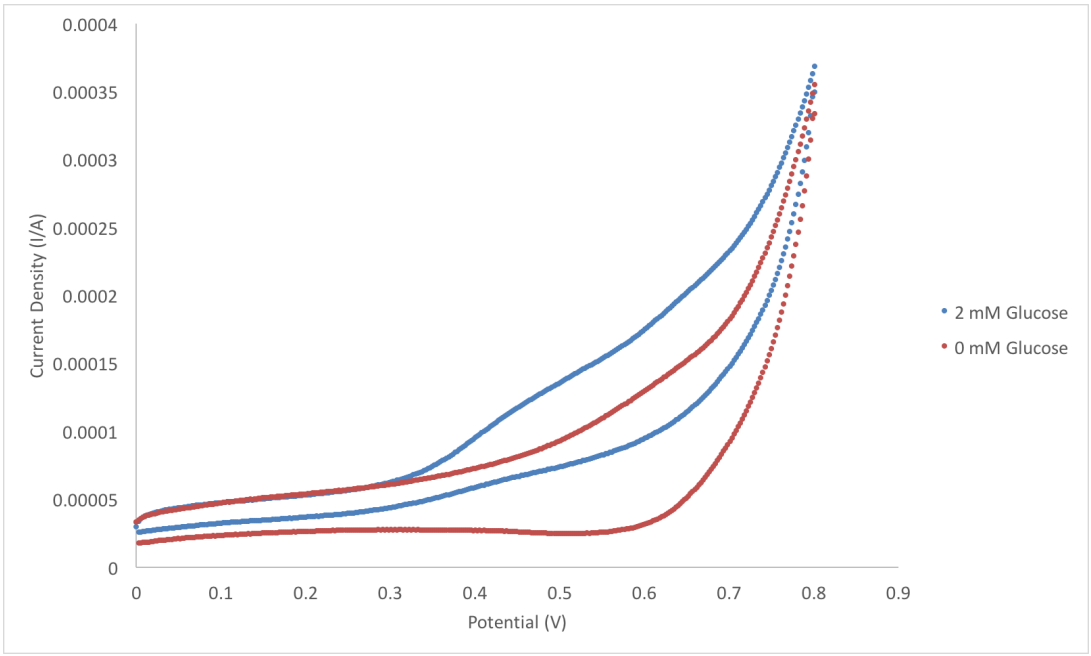

Figure 34: Cyclic voltammogram for 31.25 mM CuSO4 + H2SO4 synthesized electrode in 2 mM glucose (blue) and in 0 mM glucose (red).

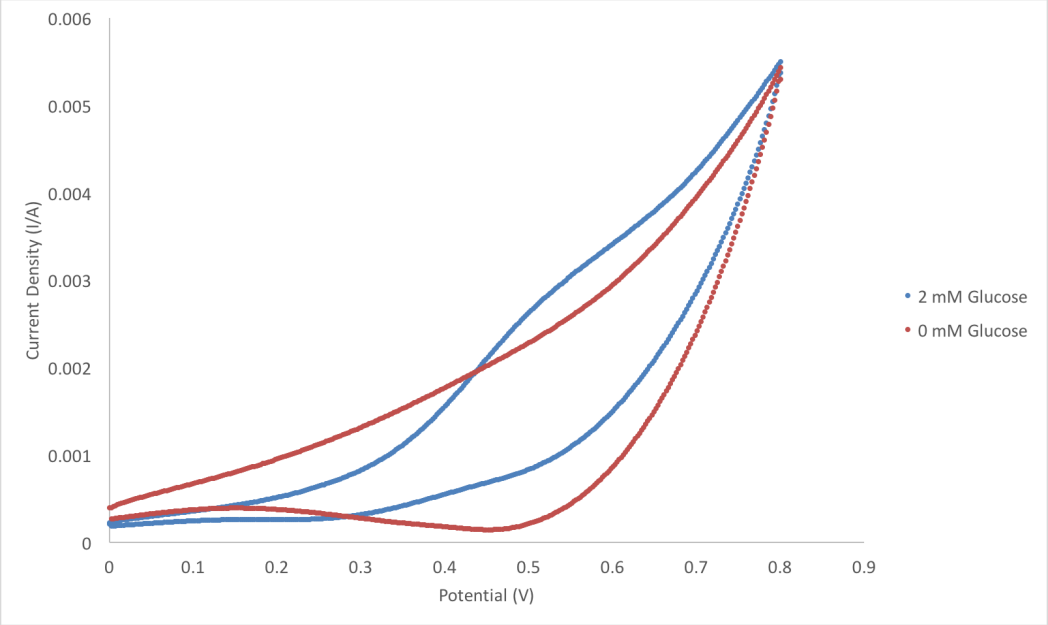

Figure 35: Cyclic voltammogram for 62.5 mM CuSO4 + H2SO4 synthesized electrode in 2 mM glucose (blue) and in 0 mM glucose (red).

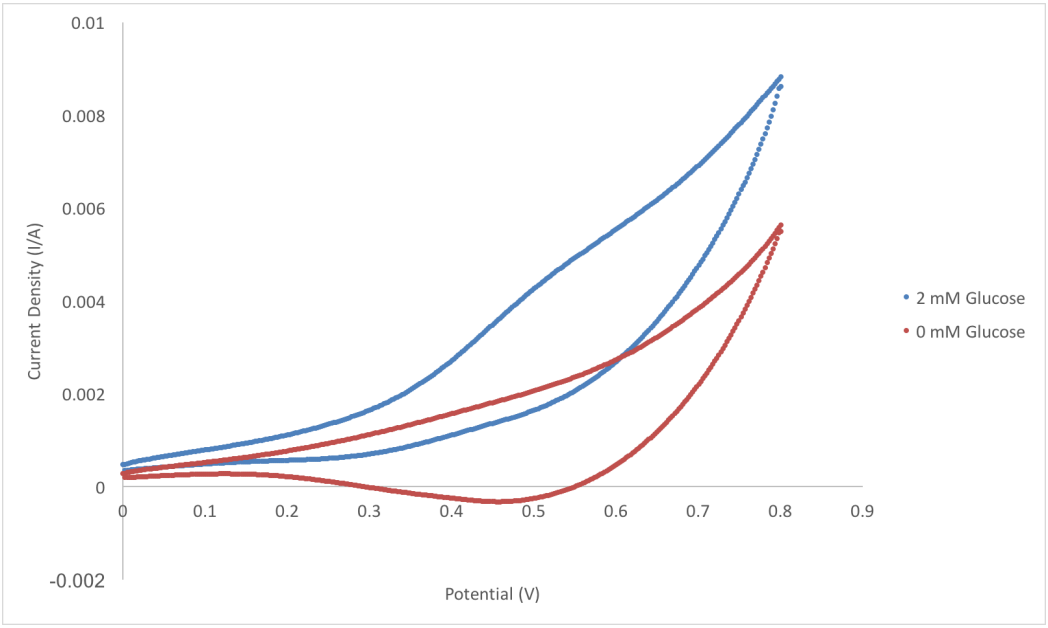

Figure 36: Cyclic voltammogram for 125 mM CuSO4 + H2SO4 synthesized electrode in 2 mM glucose (blue) and in 0 mM glucose (red).

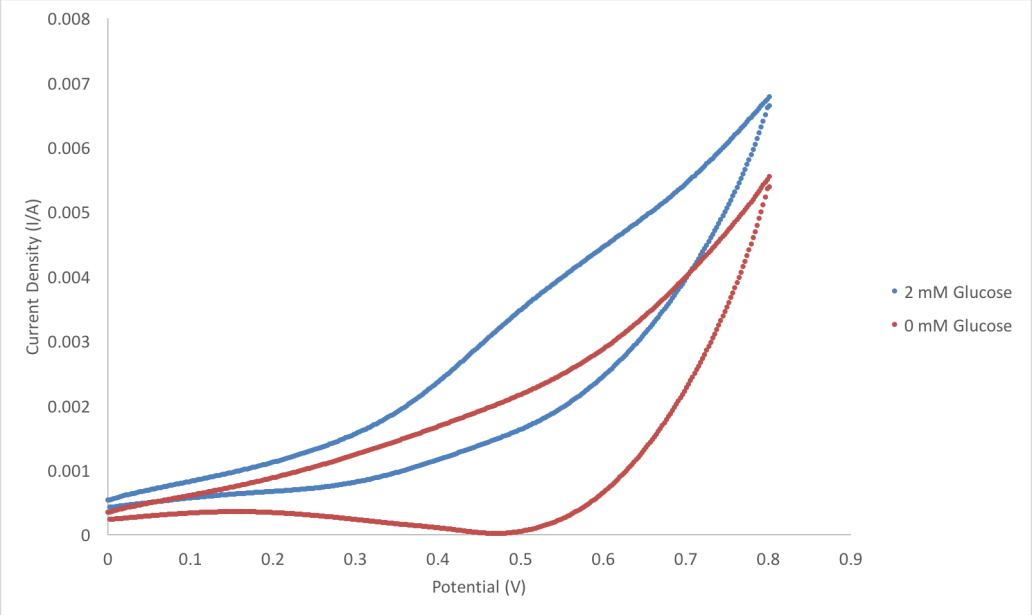

Figure 37: Cyclic voltammogram for 250 mM CuSO4 + H2SO4 synthesized electrode in 2 mM glucose (blue) and in 0 mM glucose (red).

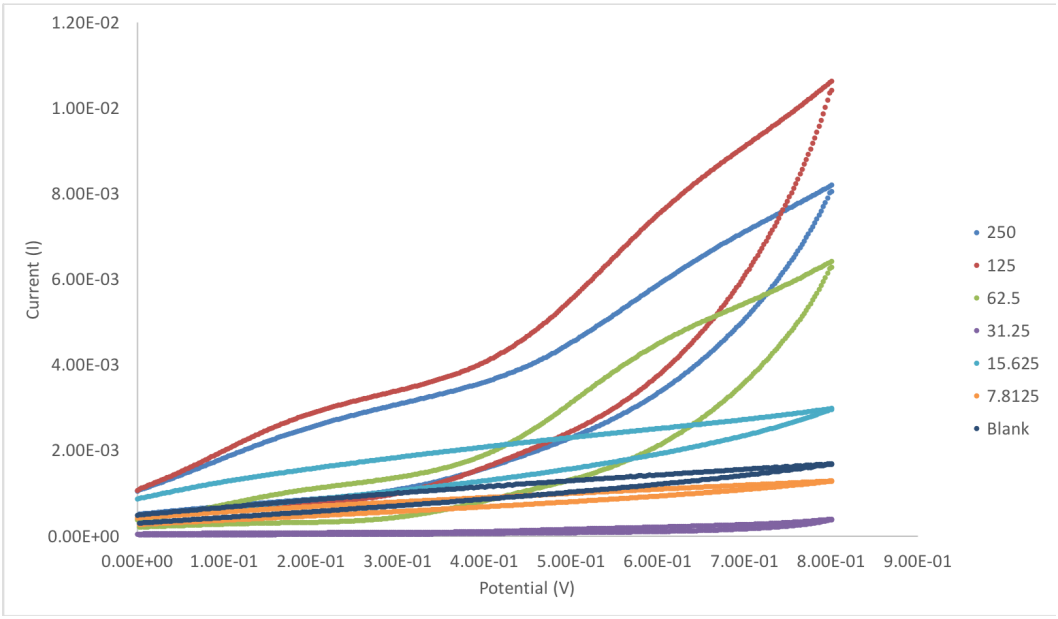

Figure 38: Cyclic voltammogram for blank (dark blue), 7.8 mM (orange), 15.6 mM (light blue), 31.3 mM (purple), 62.5 mM (green), 125 mM (red), and 250 mM (blue) in 2 mM glucose.

Appendix B: Cyclic Voltammograms for Electrodes Synthesized Under Narrow Electrolyte Concentration Range

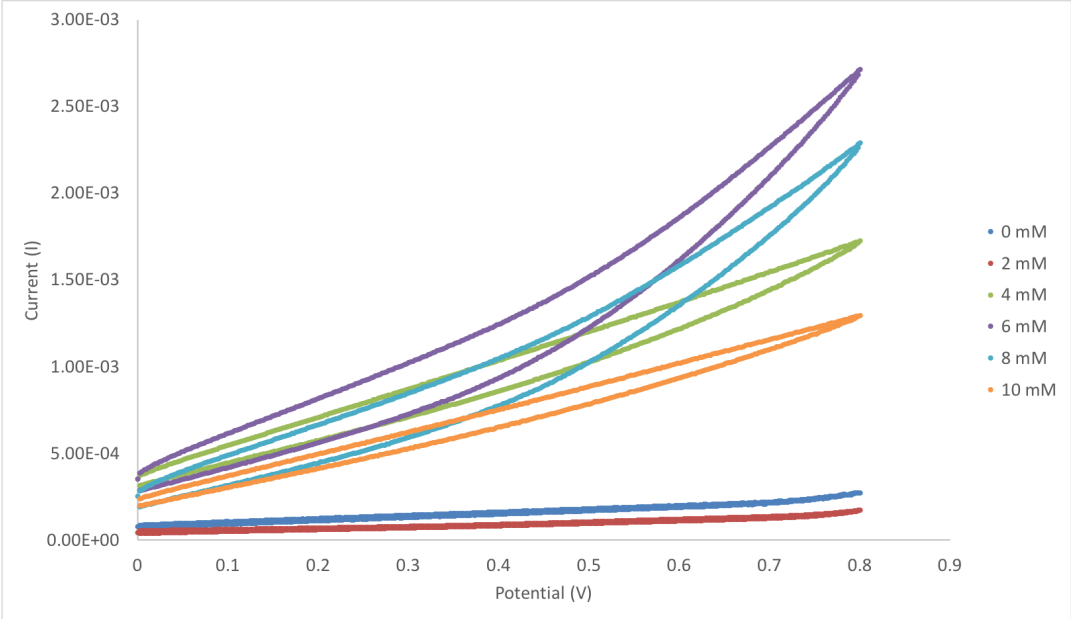

Figure 39: 30 mM electrode scanned in 0 mM (dark blue), 2 mM (red), 4 mM (green), 6 mM (purple), 8 mM (light blue), and 10 mM (orange) glucose solutions.

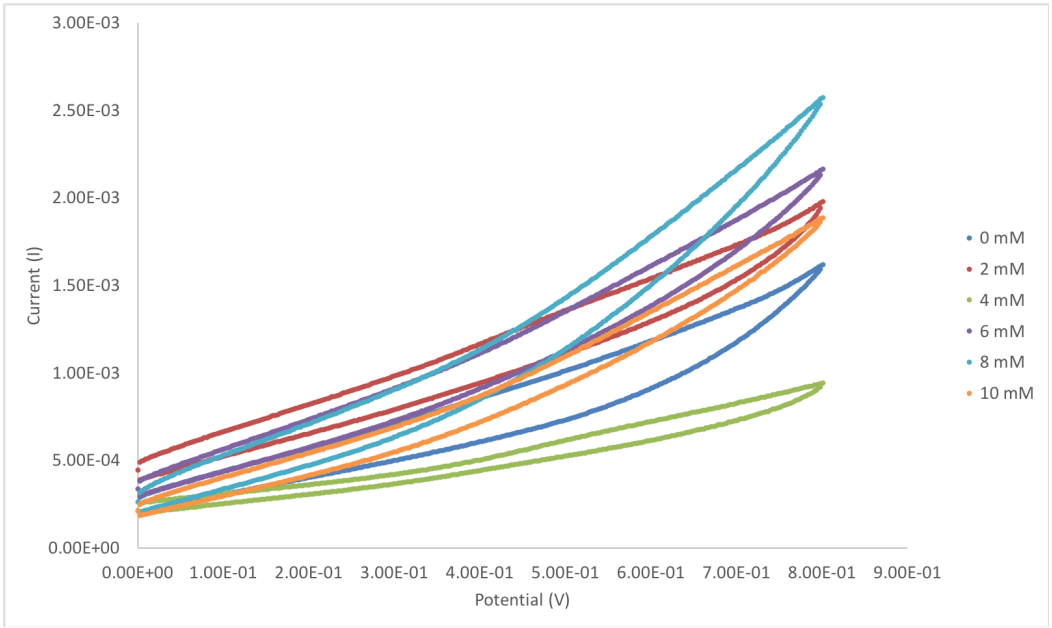

Figure 40: 40 mM electrode scanned in 0 mM (dark blue), 2 mM (red), 4 mM (green), 6 mM (purple), 8 mM (light blue), and 10 mM (orange) glucose solutions.

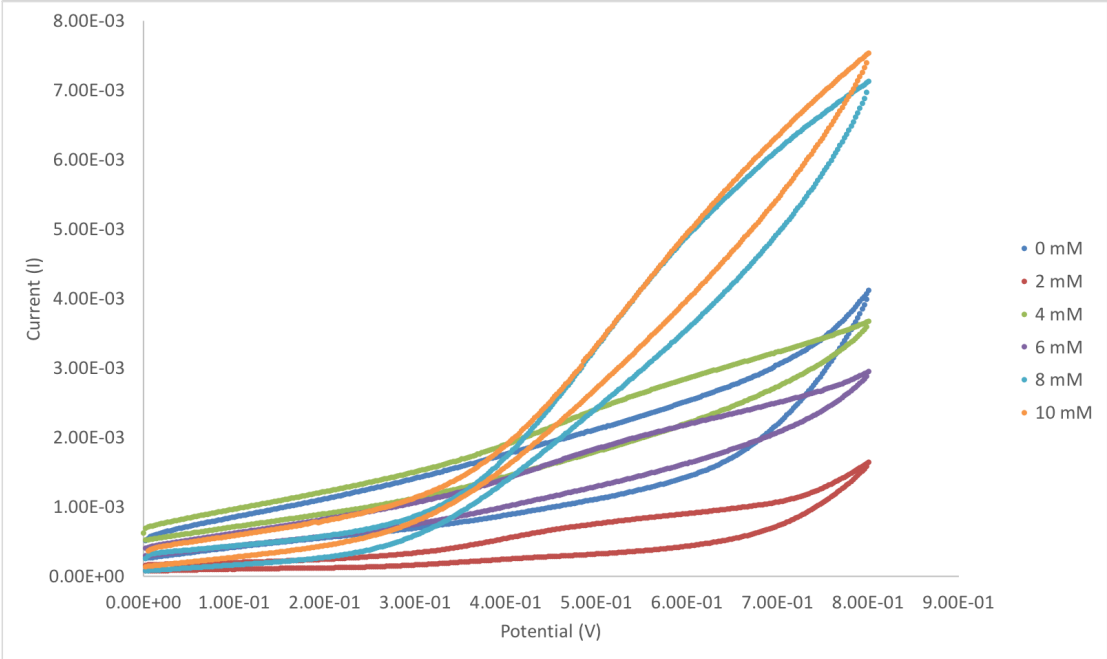

Figure 41: 60 mM electrode scanned in 0 mM (dark blue), 2 mM (red), 4 mM (green), 6 mM (purple), 8 mM (light blue), and 10 mM (orange) glucose solutions.

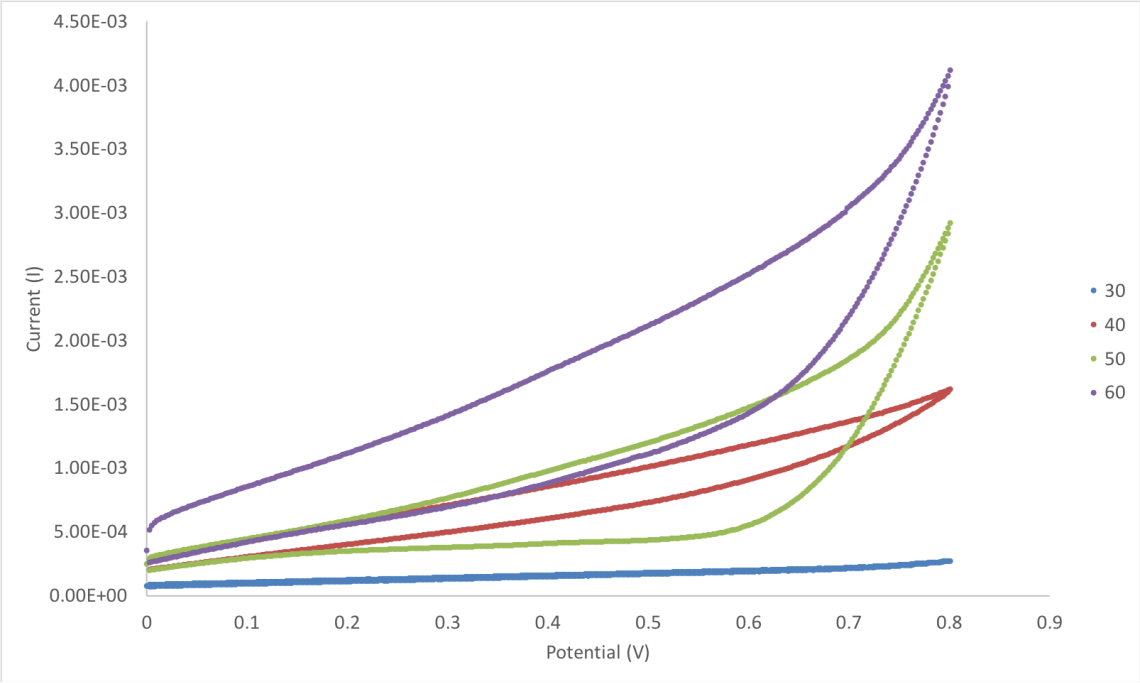

Figure 42: Cyclic voltammograms of 30 mM (blue), 40 mM (red), 50 mM (green), and 60 mM (purple) synthesized electrodes in a 0 mM glucose solution.

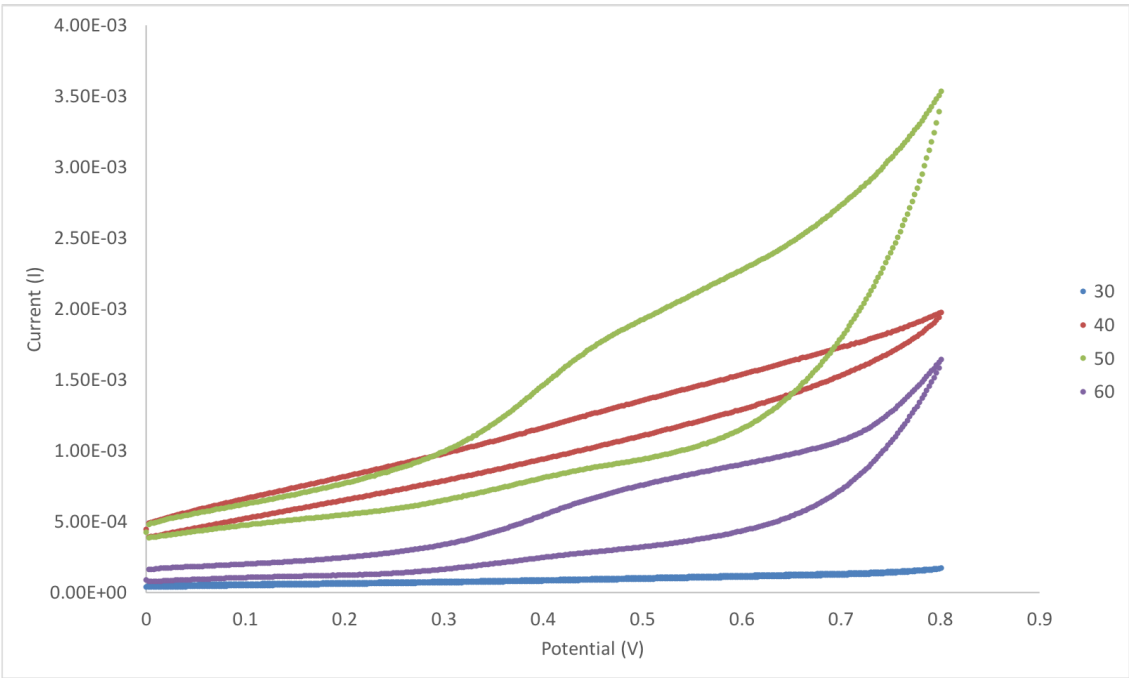

Figure 43: Cyclic voltammograms of 30 mM (blue), 40 mM (red), 50 mM (green), and 60 mM (purple) synthesized electrodes in a 2 mM glucose solution.

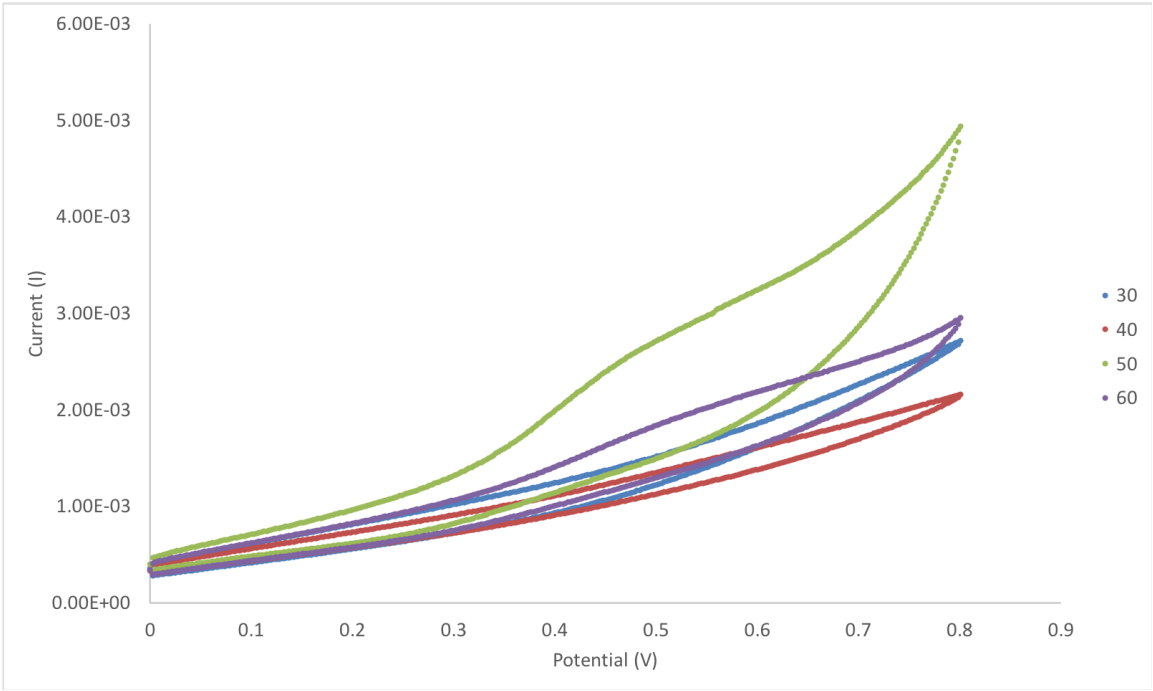

Figure 44: Cyclic voltammograms of 30 mM (blue), 40 mM (red), 50 mM (green), and 60 mM (purple) synthesized electrodes in a 6 mM glucose solution.

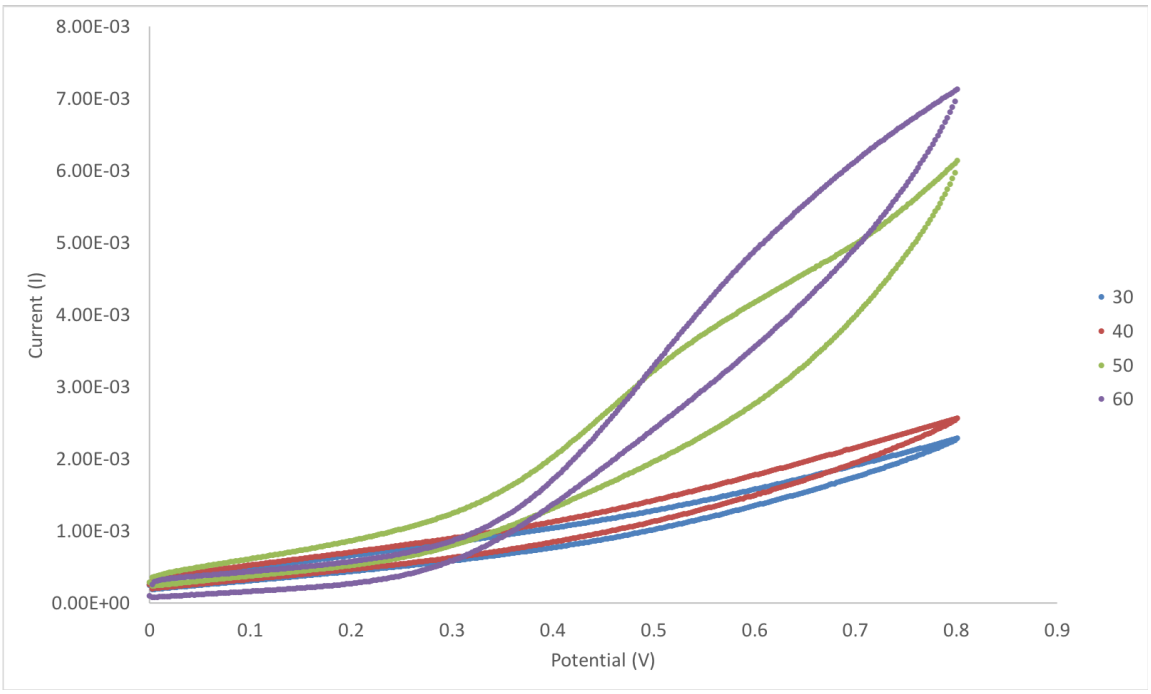

Figure 45: Cyclic voltammograms of 30 mM (blue), 40 mM (red), 50 mM (green), and 60 mM (purple) synthesized electrodes in an 8 mM glucose solution.

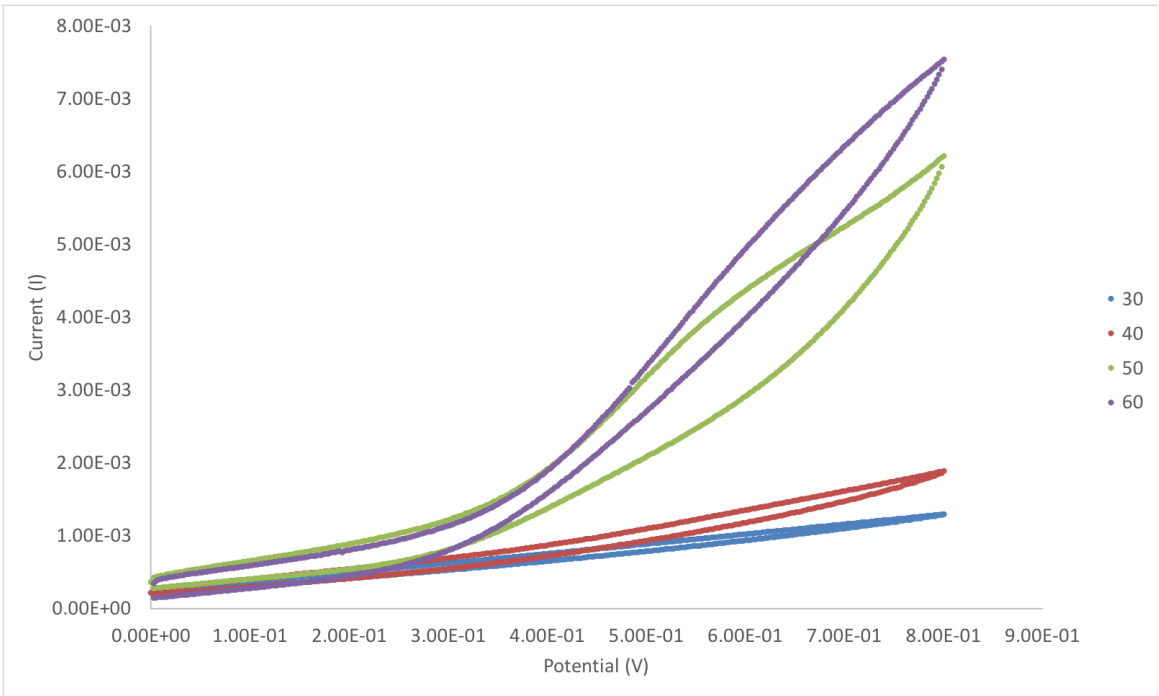

Figure 46: Cyclic voltammograms of 30 mM (blue), 40 mM (red), 50 mM (green), and 60 mM (purple) synthesized electrodes in a 10 mM glucose solution.